ODGS: 3D Scene Reconstruction from Omnidirectional Images with 3D Gaussian Splatting

Suyoung Lee[*1] **Jaeyoung Chung**[*1] **Jaeyoo Huh**[2] **Kyoung Mu Lee**[1,2]
[1]Dept. of ECE & ASRI, [2]IPAI, Seoul National University, Seoul, Korea
{esw0116, robot0321}@snu.ac.kr jaeyoo900@gmail.com kyoungmu@snu.ac.kr

Abstract

Omnidirectional (or 360-degree) images are increasingly being used for 3D applications since they allow the rendering of an entire scene with a single image. Existing works based on neural radiance fields demonstrate successful 3D reconstruction quality on egocentric videos, yet they suffer from long training and rendering times. Recently, 3D Gaussian splatting has gained attention for its fast optimization and real-time rendering. However, directly using a perspective rasterizer to omnidirectional images results in severe distortion due to the different optical properties between the two image domains. In this work, we present ODGS, a novel rasterization pipeline for omnidirectional images with geometric interpretation. For each Gaussian, we define a tangent plane that touches the unit sphere and is perpendicular to the ray headed toward the Gaussian center. We then leverage a perspective camera rasterizer to project the Gaussian onto the corresponding tangent plane. The projected Gaussians are transformed and combined into the omnidirectional image, finalizing the omnidirectional rasterization process. This interpretation reveals the implicit assumptions within the proposed pipeline, which we verify through mathematical proofs. The entire rasterization process is parallelized using CUDA, achieving optimization and rendering speeds 100 times faster than NeRF-based methods. Our comprehensive experiments highlight the superiority of ODGS by delivering the best reconstruction and perceptual quality across various datasets. Additionally, results on roaming datasets demonstrate that ODGS effectively restores fine details, even when reconstructing large 3D scenes. The source code is available on our project page.[1]

1 Introduction

With the development of VR/MR devices and robotics technologies and the increasing demands of such applications, 3D scene reconstruction has become one of the crucial tasks in computer vision. Traditional works have employed a structure-from-motion algorithm that estimates camera motion and scene geometry from multiview 2D images by finding the correspondences between images. As target 3D scenes become broader and more complex, accurate reconstruction demands a larger volume of images and increases the computational burden required for identifying correspondences. Recently, some approaches have tried to alleviate these challenges by utilizing wide-angle cameras to capture wide field-of-view images. Omnidirectional images, which provide a 360-degree field of view, are gaining increased interest because they encompass whole scenes within a single image, thereby reducing the cost of inter-image feature matching. The growing popularity of 360-degree cameras for personal video recording and the concurrent release of related datasets further facilitate the research on 3D content reconstruction from omnidirectional images.

[*]indicates equal contribution.
[1]https://github.com/esw0116/ODGS

38th Conference on Neural Information Processing Systems (NeurIPS 2024).

Such 3D reconstruction techniques [37, 51] began to be mainly studied in SLAM systems to obtain accurate camera poses with matched 3D points from monocular omnidirectional video obtained from robots. However, these models focus on restoring structural information rather than contents, and they often bypass the fine details and texture of 3D scenes. After neural radiance field (NeRF) [36] has shown outstanding 3D reconstruction performance, several works such as [10, 19, 21, 30] attempted to reconstruct 3D implicit representation from omnidirectional images. Despite showing prominent reconstruction quality, those methods commonly suffer from slow rendering and lengthy training. 3D Gaussian splatting [27], 3DGS in short, overcomes the challenges of NeRF by representing 3D contents with numerous Gaussian splats. The 3D Gaussians are initialized from the sparse point cloud obtained from the structure-from-motion and optimized through the differentiable image rasterization pipeline. Since the CUDA-implemented rasterization for 3DGS is much faster than volume rendering used in the NeRF family, 3DGS has dramatically improved rendering speed while maintaining or improving performance. Although many follow-up works have been proposed after 3DGS's success, only a few address 3DGS in the omnidirectional image domain.

In this work, we propose ODGS that aims to reconstruct high-quality 3D scenes represented by Gaussian splatting from multiple omnidirectional images. The gist of our method is designing a CUDA rasterizer that is appropriate for omnidirectional images. Specifically, we create a unit sphere from the camera origin, considering it an omnidirectional camera surface, and assume that each Gaussian is projected onto the tangent plane of the point where the vector from the camera origin to the center of the Gaussian and the unit sphere meets. Since each Gaussian is projected onto a different plane, we calculate a rotation matrix for the coordinate transformation to ensure that each Gaussian is properly projected onto its corresponding tangent plane. Then, the projected Gaussians are subsequently mapped onto the omnidirectional image plane. Our proposed rasterizer is also easily parallelizable like the original 3DGS rasterizer, demonstrating fast optimization and rendering speed. Finally, we carefully apply the densification rule to split or prune the Gaussians for omnidirectional projection. We apply a dynamic gradient threshold value for each Gaussian based on its elevation, as the azimuthal width of the projected Gaussian is stretched when transformed into an equirectangular space. We conduct comprehensive experiments comparing the reconstruction quality in various 360-degree video datasets with various environments, including egocentric and roaming, real and synthetic. The results show that ODGS achieves much faster optimization speed than existing NeRF-based methods and reconstructs the scenes with higher accuracy. Additionally, the perceptual metrics and qualitative results demonstrate that our method restores textural details more sharply.

To summarize, our contributions are three-fold:

- We introduce ODGS, a 3D reconstruction framework for omnidirectional images based on 3D Gaussian splatting, achieving 100 times faster optimization and rendering speed than NeRF-based methods.
- We present a detailed geometric interpretation of the rasterization for omnidirectional images, along with mathematical verification, and propose a CUDA rasterizer based on the interpretation.
- We comprehensively validate ODGS on various egocentric and roaming datasets, showing both more accurate reconstructed results and better perceptual quality.

2 Related works

In computer vision, ongoing research has been on creating 3D representations of the surrounding environment using multi-view images. Among them, omnidirectional images capture the surrounding space in a single image due to their wide field of view, making them increasingly popular for 3D reconstruction and mapping. Traditional structure-from-motion (SfM) algorithms [38, 42, 43] simultaneously estimate camera poses and 3D geometry structure by extracting and matching feature points across multiple images. This field has developed over many years, resulting in the release of user-friendly open libraries such as COLMAP [43] or OpenMVG [37]. Recent advancements continue to improve feature matching for spherical images [16]. In indoor environments, additional information such as room layout [2, 40, 41] and planar surfaces [14, 45] are used to promote the reconstruction quality. The geometry structures estimated from omnidirectional images are also utilized for localization [22, 28] or for simultaneous localization and mapping (SLAM) research [5, 44, 49]. The wide field of view provided by omnidirectional cameras enables the simultaneous capture of extensive spatial information, making them highly beneficial in robotic applications for environmental perception and understanding. Beyond sparse geometry structure in SfM, Multi-View Stereo (MVS) [15] supports dense reconstruction based on epipolar geometry to achieve better results. Recently, multi-view stereo techniques leveraging deep neural networks have been actively researched. [9, 32, 35] Another approach to representing 3D is by stacking multiple layers of multi-sphere images. Inspired by multi-planar images, this method facilitates the egocentric representation of scenes [1, 18]. These methods show the possibilities of 3D reconstructions using omnidirectional images, but often lack textural details for photo-realistic 3D reconstruction or limit the representation to confined spaces.

In recent 3D reconstruction research, Neural Radiance Field (NeRF) [36] has demonstrated the capability for photo-realistic novel-view synthesis, leading to studies on NeRF-based 360 image 3D reconstruction. This approach is widely used for directly reconstructing scenes in 3D [10, 17, 21, 33] or indirectly representing 3D by estimating depth [6, 8, 30]. In particular, EgoNeRF [10] is a recently published NeRF-based reconstruction method, pointing out that a typical Cartesian coordinate is not appropriate for representing a large scene with omnidirectional images. It introduces a new spherically balanced feature grid and hierarchical density adaptation during ray casting, achieving a prominent reconstruction quality. However, although NeRF-based methods have shown more realistic reconstruction than traditional techniques, they have the inherent limitation of requiring extensive time for reconstruction and rendering.

3D Gaussian splatting (3DGS) [27] is a novel 3D representation that demonstrates photo-realistic novel view synthesis while supporting fast optimization and real-time rendering. 3DGS explicitly expresses a space using a set of Gaussian primitives and quickly creates novel views through a rasterization pipeline without the time-consuming ray-casting process in NeRF. Due to its high applicability, extensive research is rapidly advancing, covering not only typical reconstruction but also sparse reconstruction [12, 55], dynamic scene reconstruction [24, 50, 52], SLAM [26, 34] and even generation [11, 46, 54]. However, 3D scene reconstruction based on omnidirectional images has been barely studied. This is partly because developing a suitable rasterizer for omnidirectional images that allows real-time rendering is challenging, and such implementations are not publicly available. 360-GS [2] is the first method that proposes omnidirectional reconstruction with 3DGS, employing a two-step strategy. However, it relies on layout-guided error correction, which limits its applicability to indoor scenes. In this paper, we present a carefully implemented CUDA rasterizer that rotates the projection plane on a unit sphere, which can efficiently optimize 3D Gaussians without any constraints or assumptions on scenes. Further, we propose a dynamic densification rule designed for a 360-degree camera from our analysis, enabling us to reconstruct high-quality scenes rapidly. We note that a few concurrent works, such as Gaussian splatting with optimal projection strategy [23] or OmniGS [31], partly share the contributions with ours.

3 Methods

3.1 Preliminary: Rasterization Process in Typical 3D Gaussian Splatting

3D Gaussian splatting (3DGS) [27] is a recently proposed 3D representation that models scenes using a set of 3D anisotropic Gaussians derived from multi-view images. It initializes the 3D Gaussians using a traditional structure-from-motion library and optimizes their properties—such as position, color, scale, rotation, and opacity—through photometric loss. In this section, we explain the rasterization pipeline for 3D Gaussians in a perspective camera as proposed by 3DGS, followed by a discussion of the differences in the rasterization process for an omnidirectional camera.

A 3D Gaussian is represented by its mean and covariance, where the covariance matrix $\mathbf{\Sigma}$ is expressed as the product of a rotation matrix $\mathbf{R}$ and a scale matrix $\mathbf{S}$ ($\mathbf{\Sigma} = \mathbf{R}\mathbf{S}\mathbf{S}^T\mathbf{R}^T$) to facilitate optimization through gradient descent. When the 3D Gaussian is projected onto the image plane of a perspective camera, the resulting distribution becomes complex since the perspective projection is not a linear transformation. Following the approach in EWA splatting [56], 3DGS approximates the projected distribution on the image plane as a 2D Gaussian. While introducing some errors, the local affine approximation simplifies the modeling of the projected 3D Gaussian, ultimately reducing computational complexity and increasing rendering speed. Based on the perspective camera projection function $\pi(\boldsymbol{\mu}) = \mathbf{K}_{1:2}\left[{}^{\mu_x}/_{\mu_z}, {}^{\mu_y}/_{\mu_z}, 1\right]^T$ with intrinsic matrix $\mathbf{K}$, the first-order approximation of the projection π is given as,

$$\mathbf{J} = \frac{\partial \pi(\boldsymbol{\mu})}{\partial \boldsymbol{\mu}} = \begin{bmatrix} \frac{f_x}{\mu_z} & 0 & -\frac{f_x \mu_x}{\mu_z^2} \\ 0 & \frac{f_y}{\mu_z} & -\frac{f_y \mu_y}{\mu_z^2} \end{bmatrix} \in \mathbb{R}^{2\times 3}, \tag{1}$$

where f_x, f_y are focal lengths of the camera and $\boldsymbol{\mu} = [\mu_x, \mu_y, \mu_z]$ is the mean vector of 3D Gaussian expressed in the camera coordinate system. As a result, the 2D Gaussian distribution on the image plane is represented with mean $\pi(\boldsymbol{\mu}) \in \mathbb{R}^2$ and covariance $\boldsymbol{\Sigma}_{\text{2D}} = \mathbf{J}\mathbf{W}\boldsymbol{\Sigma}\mathbf{W}^T\mathbf{J}^T \in \mathbb{R}^{2\times 2}$, where $\mathbf{W}$ denotes the transformation matrix from world space to camera space. The 2D Gaussian represents the intensity on the image plane and is normalized as follows to ensure the maximum value at the center becomes 1.

$$\text{For } \boldsymbol{x} \in \mathbb{R}^2, \quad G_{\text{2D}}(\boldsymbol{x}) = \exp\left(-\frac{1}{2}(\boldsymbol{x} - \pi(\boldsymbol{\mu}))^T \boldsymbol{\Sigma}_{\text{2D}}^{-1}(\boldsymbol{x} - \pi(\boldsymbol{\mu}))\right). \tag{2}$$

This bell-shaped intensity is multiplied by the Gaussian's opacity to determine the pixel-wise opacity α. After frustum culling and sorting by depth, the color of each pixel C is determined as,

$$C = \sum_{j\in N} c_j \alpha_j T_j, \quad T_j = \prod_{k=1}^{j-1}(1 - \alpha_k), \tag{3}$$

where c_j is the color of each Gaussian. This accumulation process is performed in the order of depth sorting. Each pixel is processed independently by a single GPU thread, enabling rapid rendering of 3D Gaussians into images through this rasterization process. While 3DGS describes the rasterization pipeline of 3D Gaussians for the perspective camera, a rasterization pipeline for an omnidirectional camera requires a distinct approach that regards its different optical characteristics. The following section explains our carefully designed rasterizer for the omnidirectional images.

3.2 Designing Rasterizer for Omnidirectional Images

A 360-degree camera captures all rays from the surrounding 3D environment to the camera origin and represents them on a unit sphere $\mathbb{S}^2$. We employ spherical projection or equirectangular projection (ERP) to map the projected image on the sphere $\mathbb{S}^2$ to the equirectangular space $\mathbb{R}^2$, then transform to pixel space $\mathbb{R}^2$. We describe a series of steps on how a 3D Gaussian is approximated as a 2D Gaussian in the pixel space and the feasibility of such an approximation. The gist of our rasterizer design for the omnidirectional camera is leveraging locally approximated perspective projection on $\mathbb{S}^2$ while minimizing errors.

As demonstrated in Figure 1, we follow a camera coordinate convention [4] with the z-axis forward, the x-axis to the right, and the y-axis down. We define spherical coordinates by setting the azimuth ϕ from the forward z-axis within the range $[-\pi, \pi]$ and the elevation θ from the z-x plane within the range $[-\pi/2, \pi/2]$. Projecting the mean $\boldsymbol{\mu}$ of the 3D Gaussian onto the unit sphere results in $\hat{\boldsymbol{\mu}} = \boldsymbol{\mu}/||\boldsymbol{\mu}||$, which corresponds to the azimuth $\phi_\mu = \arctan(\mu_x/\mu_z)$ and elevation $\theta_\mu = \arctan(-\mu_y/\sqrt{\mu_x^2 + \mu_z^2})$. This spherical coordinate representation (ϕ, θ) is converted into pixel space by multiplying scalar and adding center shift,

$$\pi_o(\boldsymbol{\mu}) = \left(\frac{W}{2\pi}\phi_\mu + \frac{W}{2}, -\frac{H}{\pi}\theta_\mu + \frac{H}{2}\right)^T \tag{4}$$

where W, H are the width and height of the omnidirectional image, respectively.

While finding the corresponding point of the center of 3D Gaussian on the pixel space is straightforward, calculating the covariance requires more careful consideration. We model the distribution of 3D Gaussian projected onto pixel space as a 2D Gaussian for computational efficiency and stability, following a similar approach to 3DGS. We leverage the perspective camera and local affine approximation to intuitively describe the non-linear transformation introduced by the spherical camera characteristics and the equirectangular projection. Then, we mathematically prove the correctness of the proposed method.

Let us assume a perspective camera with a unit focal length, where the image plane is tangent to the unit sphere. We rotate the perspective camera's forward direction to align with the position of the Gaussian center, $\boldsymbol{\mu}$, as shown in Figure 1 (a). The image plane is tangent to the unit sphere at $\hat{\boldsymbol{\mu}}$, the

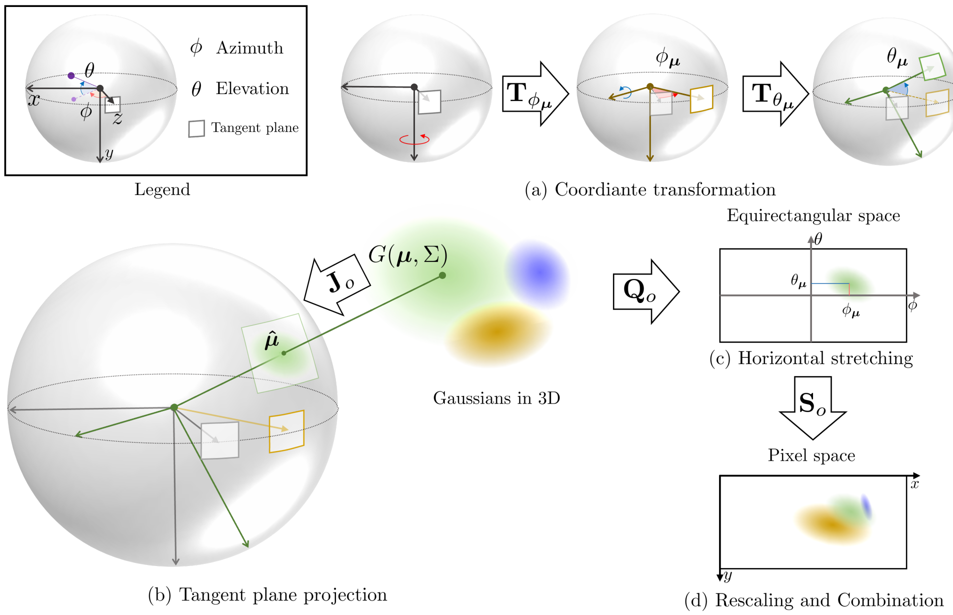

Figure 1: Illustration on rasterization process of ODGS. We describe the process of projecting a 3D Gaussian to the omnidirectional pixel space. (a) The coordinate is transformed from the original camera pose (black) to the target Gaussian (green), making the z-axis of the coordinate head towards the center of the Gaussian. (b) The Gaussian is projected onto the corresponding tangent plane. (c) The projected Gaussian is horizontally stretched when transformed into equirectangular space. (d) The Gaussian in equirectangular space is linearly transformed to the pixel space, followed by a combination with the other projected Gaussian.

point where the line from the sphere's center to the center of 3D Gaussian intersects the sphere. We define the rotation matrix of the perspective camera as $\mathbf{T}_{\boldsymbol{\mu}}$, which is accomplished in two rotations in azimuth and elevation,

$$\mathbf{T}_{\boldsymbol{\mu}} = \mathbf{T}_{\theta_\mu} \times \mathbf{T}_{\phi_\mu} = \begin{bmatrix} 1 & 0 & 0 \\ 0 & \cos\theta_\mu & \sin\theta_\mu \\ 0 & -\sin\theta_\mu & \cos\theta_\mu \end{bmatrix} \times \begin{bmatrix} \cos\phi_\mu & 0 & -\sin\phi_\mu \\ 0 & 1 & 0 \\ \sin\phi_\mu & 0 & \cos\phi_\mu \end{bmatrix}$$
$$= \begin{bmatrix} \cos\phi_\mu & 0 & -\sin\phi_\mu \\ \sin\theta_\mu \sin\phi_\mu & \cos\theta_\mu & \sin\theta_\mu \cos\phi_\mu \\ \cos\theta_\mu \sin\phi_\mu & -\sin\theta_\mu & \cos\theta_\mu \cos\phi_\mu \end{bmatrix}. \tag{5}$$

The rotation of the coordinate system helps minimize the error between the unit sphere and the image plane, while also simplifying the covariance calculation. In the rotated camera coordinate, the position of the Gaussian is represented as $\boldsymbol{\mu}_o = (0, 0, ||\boldsymbol{\mu}||)$. Thus, the Jacobian matrix from Eq. 1 is simplified as,

$$\mathbf{J}_o = \begin{bmatrix} 1/||\boldsymbol{\mu}|| & 0 & 0 \\ 0 & 1/||\boldsymbol{\mu}|| & 0 \end{bmatrix}, \tag{6}$$

because the focal length of the perspective camera is assumed to be one ($f_x = f_y = 1$). Thus, the covariance of the 3D Gaussian projected onto this tangent plane is modeled as $\mathbf{J}_o\mathbf{W}\boldsymbol{\Sigma}\mathbf{W}^T\mathbf{J}_o^T$, as shown in Figure 1 (b). We assume that the covariance of this 2D Gaussian is small enough to disregard the difference between the tangent plane and the sphere surface, allowing us to transfer it directly onto the sphere surface. Although this assumption does not generally hold, we ensure its validity through the split rule in 3DGS, which keeps the size of the Gaussian small. Next, we map the 2D covariance from the spherical surface $\mathbb{S}^2$ to the equirectangular space $(\phi, \theta) \in \mathbb{R}^2$, as described in Figure 1 (c). The equirectangular projection transforms the spherical surface onto a cylindrical map, scaling a ring at latitude θ with an initial radius of $\cos\theta$ on the sphere to a radius of 1. This projection introduces a horizontal scaling factor of $\sec\theta$, leading to increased distortion as θ approaches the poles. We incorporate the distortion through $\mathbf{Q}_o$, and then we rescale the covariance to the pixel space by applying the appropriate scaling factors $\mathbf{S}_o$,

$$\mathbf{Q}_o = \begin{bmatrix} \sec\theta_\mu & 0 \\ 0 & 1 \end{bmatrix}, \quad \mathbf{S}_o = \begin{bmatrix} W/2\pi & 0 \\ 0 & H/\pi \end{bmatrix}. \tag{7}$$

As a result, the final Jacobian matrix is given as,

$$\mathbf{J}_{omni} = \mathbf{S}_o \mathbf{Q}_o \mathbf{J}_o \mathbf{T}_{\boldsymbol{\mu}} = \begin{bmatrix} \frac{W}{2\pi||\boldsymbol{\mu}||} \sec\theta_\mu \cos\phi_\mu & 0 & -\frac{W}{2\pi||\boldsymbol{\mu}||} \sec\theta_\mu \sin\phi_\mu \\ \frac{H}{\pi||\boldsymbol{\mu}||} \sin\theta_\mu \sin\phi_\mu & \frac{H}{\pi||\boldsymbol{\mu}||} \cos\theta_\mu & \frac{H}{\pi||\boldsymbol{\mu}||} \sin\theta_\mu \cos\phi_\mu \end{bmatrix}, \tag{8}$$

where the final 2D covariance is presented as $\boldsymbol{\Sigma}_{\text{2D},o} = \mathbf{J}_{omni} \mathbf{W} \boldsymbol{\Sigma} \mathbf{W}^T \mathbf{J}_{omni}^T$ We verify the correctness of the derived method by directly differentiating the equirectangular projection function π_o in Eq. 4, yielding the same result $\mathbf{J}_{omni} = \frac{\partial \pi_o(\boldsymbol{\mu})}{\partial \boldsymbol{\mu}}$ as detailed in Appendix A.2.

As a result of the series of steps, the final 2D covariance is used for rendering the image, as described in Eq. 2 and Eq. 3. One key difference is that, instead of performing frustum-shaped culling as in perspective cameras, we perform culling in a spherical shell. The rasterization pipeline is fully differentiable and implemented in CUDA, which can be used as a typical 3DGS. The detailed gradient calculations through back-propagation are provided in Appendix A.3.

3.3 Densification Policy for Omnidirectional Images

Due to the characteristic of equirectangular projection, a 3D Gaussian can be rendered in different shapes depending on its relative elevation to the camera; Gaussians near the poles are drawn larger. Therefore, we propose a dynamic densification strategy specifically designed for omnidirectional images. While the original method uses a pre-defined gradient threshold for densifying Gaussians, we apply a varying gradient threshold τ_μ according to the elevation angle θ_μ as,

$$\tau_\mu = \tau_{\text{min}} + (1 - \cos\theta_\mu) \times (\tau_{\text{max}} - \tau_{\text{min}}), \tag{9}$$

which mitigates excessive densification of Gaussians near the poles.

4 Experiments

4.1 Experiment Details

Datasets We evaluate our method on three egocentric datasets (OmniBlender, Ricoh360, OmniPhotos) and three roaming datasets (360Roam, OmniScenes, 360VO) to show its superiority regardless of domain. First, EgoNeRF [10] released OmniBlender and Ricoh360, which have different characteristics. OmniBlender contains 11 synthetic scenes generated with an omnidirectional rendering engine in Blender [13], with four indoor and seven outdoor scenes. The images were captured by rotating in a circular motion while ascending, each with a resolution of 2000×1000. Each scene in OmniBlender consists of 25 training and test images. Ricoh360 contains 12 real-world omnidirectional outdoor scenes captured by rotating in place in a cross-shaped pattern. Each scene consists of 50 training images and 50 testing images with a resolution of 1920×960. OmniPhotos [3] has released 10 real-world omnidirectional scenes captured by rotating in a circular motion with a commercial 360-degree camera on a selfie stick. Each scene has 71 to 91 images with a size of 3840×1920. In our experiment, we resize them to half resolution 1920×960, and we use 20% of images for the test.

For the roaming scenarios, we utilize several multi-view omnidirectional datasets, which were not originally released for 3D reconstruction tasks. 360Roam [21] dataset consists of 10 real-world indoor scenes captured by Insta360camera. Each scene has 71 to 215 omnidirectional images with size 6080×3040, and we resize them to 2048×1024. OmniScenes [28] is originally made for assessing the quality of visual localization of omnidirectional images in harsh conditions. Since it is proposed to measure the robustness of visual localization algorithms, it contains significant scene changes, motion blur, or some visual artifacts such as jpeg compression. We use the released version 1.1, which includes 7 real-world indoor captured scenes in resolution 1920×960. 360VO [20] is a simulation dataset for evaluating the localization and mapping algorithms in the robotics field. It contains 10 virtual outdoor road scenes, where each scene has 2000 images with size 1920×960.

Table 1: Quantitative comparison of 3D reconstruction methods on various datasets. The best metric for each dataset is written in **bold**. Our method shows the best performance on almost all settings regardless of optimization time, with the fastest rendering speed.

Dataset	Methods	10 min PSNR↑	10 min SSIM↑	10 min LPIPS↓	100 min PSNR↑	100 min SSIM↑	100 min LPIPS↓	Time↓ (sec.)
OmniBlender	NeRF(P)	19.20	0.6124	0.5359	20.04	0.6092	0.4949	62.71
	3DGS(P)	29.36	0.8770	0.1400	21.19	0.7528	0.3021	0.112
	TensoRF	25.36	0.7249	0.3855	26.08	0.7416	0.3170	10.77
	EgoNeRF	28.29	0.8309	0.2194	30.89	0.8934	0.1260	23.78
	ODGS	**32.76**	**0.9234**	**0.0469**	**33.05**	**0.9229**	**0.0343**	**0.028**
Ricoh360	NeRF(P)	14.33	0.5616	0.5794	16.16	0.5617	0.5716	62.46
	3DGS(P)	**25.12**	0.7932	0.2397	22.07	0.7228	0.3218	0.132
	TensoRF	23.35	0.6812	0.5200	23.97	0.6936	0.4653	10.30
	EgoNeRF	24.74	0.7467	0.3243	25.49	0.7737	0.2825	23.89
	ODGS	24.94	**0.8135**	**0.1489**	**26.27**	**0.8462**	**0.1051**	**0.026**
OmniPhotos	NeRF(P)	18.14	0.6158	0.5514	20.80	0.6388	0.4772	62.08
	3DGS(P)	25.61	0.8310	0.2100	23.30	0.7859	0.2670	0.110
	TensoRF	22.78	0.6841	0.5089	23.73	0.7038	0.4467	9.707
	EgoNeRF	25.20	0.7722	0.2662	26.90	0.8349	0.1766	23.88
	ODGS	**26.24**	**0.8704**	**0.1108**	**27.04**	**0.8878**	**0.0875**	**0.028**
360Roam	NeRF(P)	15.07	0.6848	0.4839	15.26	0.6813	0.5025	62.98
	3DGS(P)	20.17	0.7001	0.3536	19.34	0.6576	0.3837	0.104
	TensoRF	18.00	0.5988	0.7488	18.12	0.5895	0.7133	9.052
	EgoNeRF	20.45	0.6358	0.5334	**21.18**	0.6718	0.4444	24.03
	ODGS	**21.08**	**0.7066**	**0.3003**	20.85	**0.7111**	**0.2254**	**0.029**
OmniScenes	NeRF(P)	15.69	0.7218	0.4546	15.98	0.6890	0.4914	62.90
	3DGS(P)	23.61	0.8444	0.2835	17.14	0.7119	0.3906	0.194
	TensoRF	23.58	0.8118	0.3534	24.21	0.8208	0.3091	8.100
	EgoNeRF	22.78	0.7997	0.3463	**24.76**	0.8313	0.2623	23.66
	ODGS	**24.42**	**0.8526**	**0.1391**	24.51	**0.8505**	**0.1282**	**0.032**
360VO	NeRF(P)	15.71	0.6186	0.4949	17.78	0.6373	0.5064	61.97
	3DGS(P)	22.87	0.7861	0.2970	22.73	0.7822	0.3061	0.091
	TensoRF	19.74	0.6543	0.5876	20.31	0.6721	0.5640	7.815
	EgoNeRF	22.47	0.7325	0.4342	23.78	0.7677	0.3680	23.96
	ODGS	**24.63**	**0.8245**	**0.2175**	**26.68**	**0.8694**	**0.1264**	**0.026**

We uniformly select 200 images for each sequence for training and testing. Since these datasets do not split the train and test images, we conducted our experiment by dividing them by 4:1 for train and test, respectively. We note that all datasets have CC-BY-4.0 licenses. Although some datasets provide camera poses and dense point clouds, we run the structure-from-motion, specifically OpenMVG [37], on all the datasets and use obtained poses and point clouds for our experiment.

Implementation details Our framework is basically built with PyTorch [39], but we manually implement the omnidirectional rasterizer using the CUDA kernel. All experiments, including optimization and inference time measurements, are conducted using a single NVIDIA RTX A6000 GPU. We describe the optimization arguments in the Appendix A.1.

4.2 Experiment Results

Baselines With no available code for 3DGS on omnidirectional images at the time of our experiments, we compare our method with NeRF-based methods, specifically TensoRF [7] and EgoNeRF [10]. We also convert omnidirectional images into perspective images to compare the typical 3D reconstruction methods, NeRF [36] and 3DGS [27]. Specifically, we transform the omnidirectional images into six perspective images using cubemap decomposition, popularly used in many

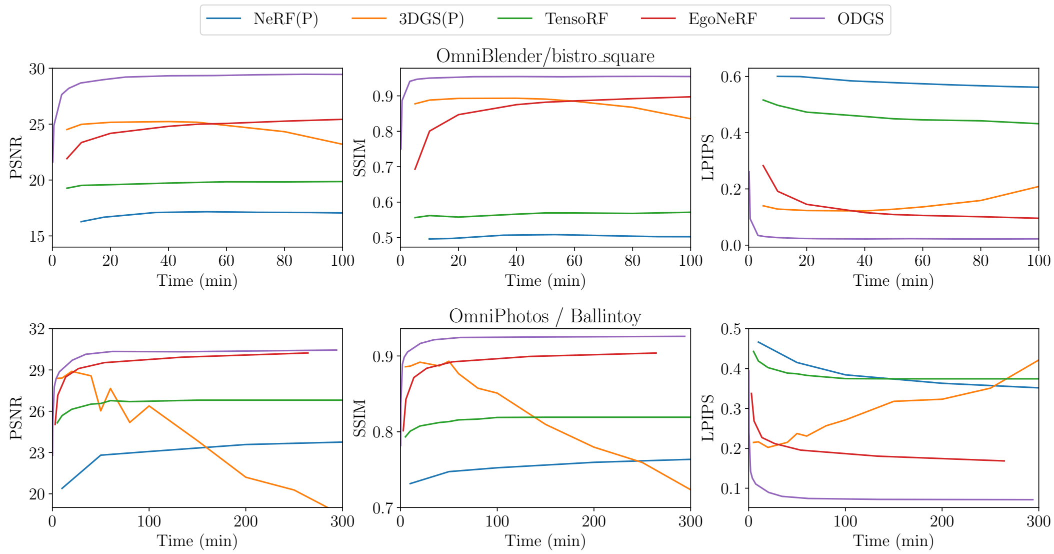

Figure 2: Changes of PSNR, SSIM, and LPIPS according to the optimization time for each method. ODGS shows the best result as well as the highest convergence speed in both scenes.

studies involving 360-degree cameras [25, 47]. The six decomposed images compose a cube-shaped surface and we calculate the corresponding camera pose of each surface. For inference, the six views for each face in the cube are rendered and then combined into an omnidirectional image.

Quantitative comparison To ensure the experiment's fairness and highlight the efficiency of our method, all methods were evaluated after optimizing the model with the same amount of time. We evaluate the performance of all methods at 10 and 100 minutes of training time, measured in wall-clock time. For evaluation metric, we use PSNR (dB), SSIM [48], and LPIPS [53] for comparing reconstruction quality, where AlexNet [29] backbone is used for measuring LPIPS. Table 1 shows the quantitative performance comparison and rendering time (seconds) for all datasets. The (P) mark in the method column indicates those methods are trained with converted perspective images. Our results show dominant results on all metrics, including inference time. NeRF and TensoRF, which use a grid based on a Cartesian coordinate system, encounter difficulties representing large scenes, resulting in poor quantitative metrics. EgoNeRF, which introduces a spherical balanced grid to mitigate the challenge, shows better quality than TensoRF but still needs better perceptual metrics. Also, these methods require more than a second to render a single omnidirectional image for an arbitrary viewpoint, which is impractical for real scenarios. Meanwhile, 3DGS with perspective images shows the best results except ours when optimized for 10 minutes, but severely suffers from overfitting and gets worse results after 100 minutes of optimization. In terms of rendering time, despite reporting faster speed than NeRF-based models, original 3DGS takes longer than typical perspective image rendering because it involves non-linear warping of each image when stitching six images to create one omnidirectional image. ODGS, in contrast, outperforms the other methods in image reconstruction quality and rendering speed. The outstanding results for SSIM and LPIPS imply that our method generates images with accurate structure and prominent perceptual quality.

Figure 2 shows the change of PSNR, SSIM, and LPIPS depending on the optimization time for two example scenes. We note that we stopped training NeRF and TensoRF at 100 and 200 minutes, respectively, since their performances converged. Our method shows the fastest optimization speed in both scenes while maintaining the highest score regardless of optimization time. Typical NeRF and TensoRF recorded significantly lower results than ours, verifying that the Cartesian coordinate is inappropriate for radially extending rays. EgoNeRF shows comparable PSNR with ours in *Ballintoy*, but needs a long optimization time. We attribute the fast optimization of ODGS to two aspects. First, while NeRF-based methods use an implicit representation that embeds the scene into a neural network, 3DGS employs explicit representation and directly moves or morphs the elements to optimize the model. Also, 3DGS exploits the position of SfM point clouds, which can serve as a good initialization point for optimizing Gaussian splats. 3DGS (P), on the other hand, shows high vulnerability to

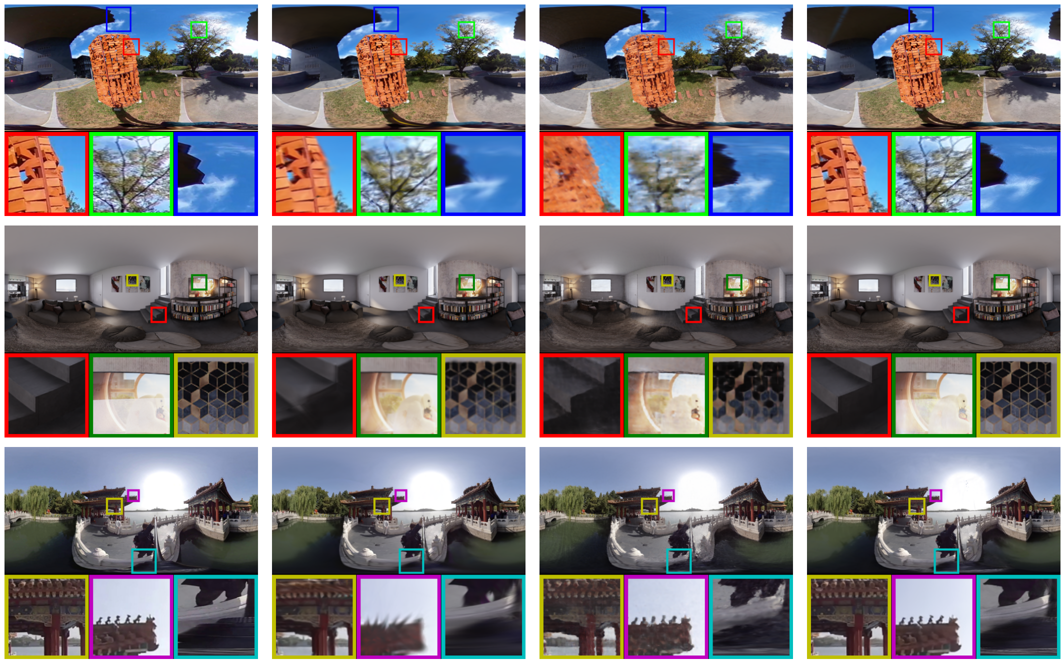

(a) Ground truth (b) 3DGS(P) [27] (c) EgoNeRF [10] (d) ODGS

Figure 3: Qualitative comparisons in the egocentric scenes (10 min.). Each scene is brought from Ricoh360, OmniBlender, and OmniPhotos, respectively. *Best viewed when zoomed in.*

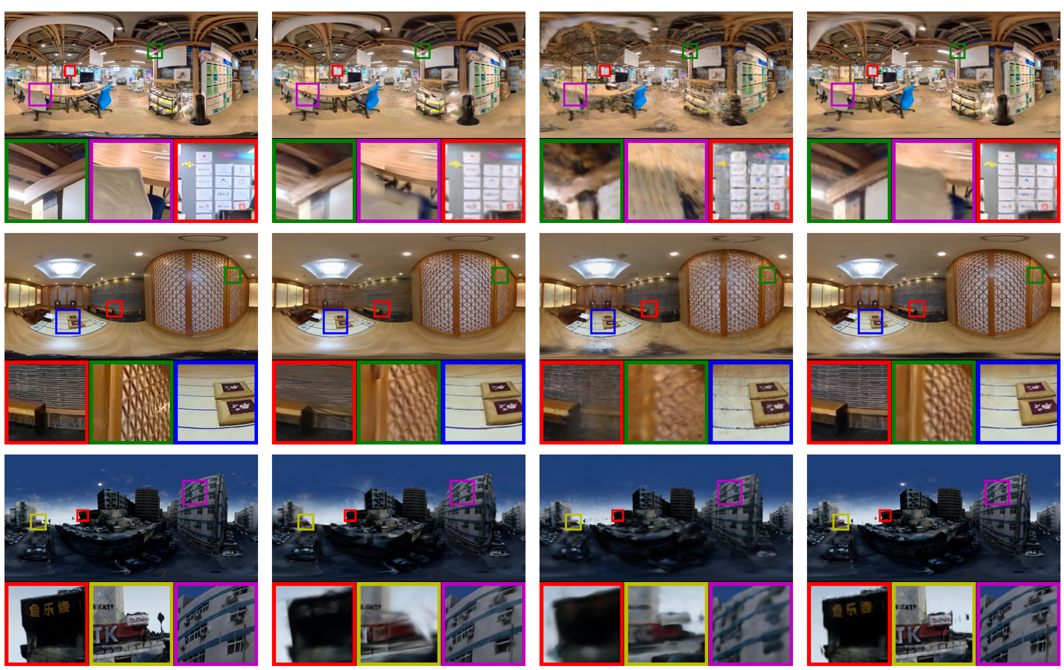

(a) Ground truth (b) 3DGS(P) [27] (c) EgoNeRF [10] (d) ODGS

Figure 4: Qualitative comparisons in the roaming scenes (10 min.). Each scene is brought from 360Roam, OmniScenes, and 360VO, respectively. *Best viewed when zoomed in.*

overfitting. We believe the phenomenon happens because of the weak correlation among the six faces of the cubemap after decomposition. Since there is no overlap between the six faces, 3DGS is optimized six times independently for faces facing the same direction. Therefore, even with the same input, the amount of information used is significantly reduced, causing overfitting to occur quickly.

Qualitative comparison We also visually compare our method with the other methods in various scenes. Figure 3 shows the samples of reconstructed images from egocentric datasets. We note that the images in the figure are rendered at 10 minutes of training. The images from EgoNeRF are blurry and contain some artifacts, such as stripe lines or checkerboard patterns, which appear prominent near the edges. The model is not sufficiently optimized to render the sharp image details. 3DGS trained with the cubemap perspective images sometimes show sharp reconstruction contents, such as a cubic pattern of a frame in the middle row (yellow boundary) but often include unintended projected Gaussian splats that cause image distortion. We attribute the phenomenon to the rapid overfitting properties of perspective 3DGS. In contrast, our model successfully reconstructs sharp details in the images. The superiority of ODGS becomes more noticeable in the roaming dataset, as shown in Figure 4. Although EgoNeRF proposes a balanced grid for egocentric video, it cannot maintain a uniform ray density for every grid if the camera wanders inside a large environment. As a result, the scene pattern is often completely lost, creating completely different results, and the overall reconstruction quality deteriorates. While perspective 3DGS shows better quality than EgoNeRF, it often misses some objects or structures where the adjacent faces of the cube meet. For instance, in the top row, there is an inverted Y-shaped artifact instead of a chair in a purple patch. This happens because the chair is located where the three sides of the cube meet, and the object is not made from any of the sides. ODGS overcomes the challenge by optimizing the Gaussian using the whole image and showing prominent performance on both egocentric and roaming datasets.

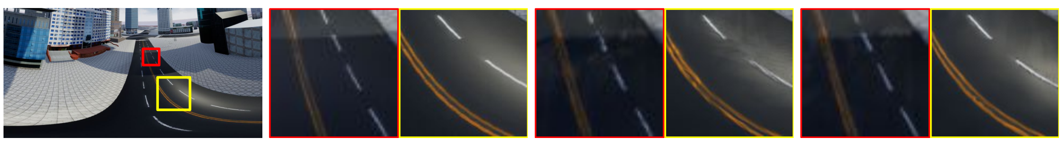

(a) Ground truth(full) (b) Ground truth (c) Static threshold (d) Dynamic threshold

Figure 5: Qualitative comparison of rendered images according to the Gaussian densification policy during optimization.

Ablation Study: Dynamic Densification Strategy for Omnidirectional Images We qualitatively compare and display the results in Figure 5 when applying the proposed dynamic densification rule proposed in Section 3.3. As shown in the figure, the lanes appear split, with artifact-like patterns emerging on the road due to static densification, as employed in the original 3DGS work [27]. Conversely, our densification strategy significantly enhances the model's representation power, leading to markedly more accurate rasterization results.

5 Conclusion

In this work, we propose a new method called ODGS, specifically designed to reconstruct 3D scenes from omnidirectional images using 3D Gaussian splatting. To optimize 3D Gaussian splatting in the omnidirectional image domain, we introduce a new rasterizer that appropriately models the equirectangular projection from the 3D space to the image. Specifically, we define a tangent plane for each Gaussian and project the Gaussian into the plane, followed by horizontal stretching and rescaling to the pixel space. Compared to the state-of-the-art NeRF-based methods, ODGS shows about 100 times faster optimization and rendering speed, which allows the user to synthesize the novel view in real-time. Furthermore, ODGS shows the best reconstruction performance for various input images, including egocentric and roaming scenes, indoors and outdoors.

Limitations and future work ODGS still relies on local affine approximation when projecting a Gaussian splat to the camera surface. Equirectangular projection is not a linear transformation, and straight lines in the 3D space should be expressed as curves in the omnidirectional image. However, a 3D Gaussian is approximated as a 2D Gaussian, leading to errors that produce artifacts in the rendered image. Adopting a more accurate distribution for spherically projected Gaussians can reduce errors and enhance the efficiency of the framework.

Acknowledgements

This work was supported in part by the IITP grants [No.2021-0-01343, Artificial Intelligence Graduate School Program (Seoul National University), No. 2021-0-02068, and No.2023-0-00156], the NRF grant [No. 2021M3A9E4080782] funded by the Korea government (MSIT), and the SNU-LG AI Research Center.

References

[1] Benjamin Attal, Selena Ling, Aaron Gokaslan, Christian Richardt, and James Tompkin. Matryodshka: Real-time 6dof video view synthesis using multi-sphere images. In *ECCV*, 2020.

[2] Jiayang Bai, Letian Huang, Jie Guo, Wen Gong, Yuanqi Li, and Yanwen Guo. 360-gs: Layout-guided panoramic gaussian splatting for indoor roaming. *arXiv preprint arXiv:2402.00763*, 2024.

[3] Tobias Bertel, Mingze Yuan, Reuben Lindroos, and Christian Richardt. Omniphotos: casual 360 vr photography. *ACM TOG*, 2020.

[4] Gary Bradski. The opencv library. *Dr. Dobb's Journal: Software Tools for the Professional Programmer*, 25(11):120–123, 2000.

[5] David Caruso, Jakob Engel, and Daniel Cremers. Large-scale direct slam for omnidirectional cameras. In *IROS*, 2015.

[6] Wenjie Chang, Yueyi Zhang, and Zhiwei Xiong. Depth estimation from indoor panoramas with neural scene representation. In *CVPR*, 2023.

[7] Anpei Chen, Zexiang Xu, Andreas Geiger, Jingyi Yu, and Hao Su. Tensorf: Tensorial radiance fields. In *ECCV*, 2022.

[8] Rongsen Chen, Fang-Lue Zhang, Simon Finnie, Andrew Chalmers, and Taehyun Rhee. Casual 6-dof: free-viewpoint panorama using a handheld 360 camera. *IEEE TVCG*, 2022.

[9] Ching-Ya Chiu, Yu-Ting Wu, I Shen, Yung-Yu Chuang, et al. 360mvsnet: Deep multi-view stereo network with 360deg images for indoor scene reconstruction. In *WACV*, 2023.

[10] Changwoon Choi, Sang Min Kim, and Young Min Kim. Balanced spherical grid for egocentric view synthesis. In *CVPR*, 2023.

[11] Jaeyoung Chung, Suyoung Lee, Hyeongjin Nam, Jaerin Lee, and Kyoung Mu Lee. Luciddreamer: Domain-free generation of 3d gaussian splatting scenes. *arXiv preprint arXiv:2311.13384*, 2023.

[12] Jaeyoung Chung, Jeongtaek Oh, and Kyoung Mu Lee. Depth-regularized optimization for 3d gaussian splatting in few-shot images. In *CVPR Workshop*, 2024.

[13] Blender Online Community. *Blender - a 3D modelling and rendering package*. Blender Foundation, Stichting Blender Foundation, Amsterdam, 2018.

[14] Marc Eder, Pierre Moulon, and Li Guan. Pano popups: Indoor 3d reconstruction with a plane-aware network. In *3DV*, 2019.

[15] Yasutaka Furukawa, Carlos Hernández, et al. Multi-view stereo: A tutorial. *Foundations and Trends® in Computer Graphics and Vision*, 2015.

[16] Christiano Gava, Vishal Mukunda, Tewodros Habtegebrial, Federico Raue, Sebastian Palacio, and Andreas Dengel. Sphereglue: Learning keypoint matching on high resolution spherical images. In *CVPR*, 2023.

[17] Kai Gu, Thomas Maugey, Sebastian Knorr, and Christine Guillemot. Omni-nerf: neural radiance field from 360 image captures. In *ICME*, 2022.

[18] Tewodros Habtegebrial, Christiano Gava, Marcel Rogge, Didier Stricker, and Varun Jampani. Somsi: Spherical novel view synthesis with soft occlusion multi-sphere images. In *CVPR*, 2022.

[19] Ching-Yu Hsu, Cheng Sun, and Hwann-Tzong Chen. Moving in a 360 world: Synthesizing panoramic parallaxes from a single panorama. *arXiv preprint arXiv:2106.10859*, 2021.

[20] Huajian Huang and Sai-Kit Yeung. 360vo: Visual odometry using a single 360 camera. In *ICRA*, 2022.

[21] Huajian Huang, Yingshu Chen, Tianjia Zhang, and Sai-Kit Yeung. Real-time omnidirectional roaming in large scale indoor scenes. In *SIGGRAPH Asia 2022 Technical Communications*, 2022.

[22] Huajian Huang, Changkun Liu, Yipeng Zhu, Hui Cheng, Tristan Braud, and Sai-Kit Yeung. 360loc: A dataset and benchmark for omnidirectional visual localization with cross-device queries. *arXiv preprint arXiv:2311.17389*, 2023.

[23] Letian Huang, Jiayang Bai, Jie Guo, Yuanqi Li, and Yanwen Guo. On the error analysis of 3d gaussian splatting and an optimal projection strategy. In *ECCV*, 2024.

[24] Yi-Hua Huang, Yang-Tian Sun, Ziyi Yang, Xiaoyang Lyu, Yan-Pei Cao, and Xiaojuan Qi. Sc-gs: Sparse-controlled gaussian splatting for editable dynamic scenes. *arXiv preprint arXiv:2312.14937*, 2023.

[25] Hyeonjoong Jang, Andreas Meuleman, Dahyun Kang, Donggun Kim, Christian Richardt, and Min H Kim. Egocentric scene reconstruction from an omnidirectional video. *ACM ToG*, 2022.

[26] Nikhil Keetha, Jay Karhade, Krishna Murthy Jatavallabhula, Gengshan Yang, Sebastian Scherer, Deva Ramanan, and Jonathon Luiten. Splatam: Splat, track & map 3d gaussians for dense rgb-d slam. *arXiv preprint arXiv:2312.02126*, 2023.

[27] Bernhard Kerbl, Georgios Kopanas, Thomas Leimkühler, and George Drettakis. 3d gaussian splatting for real-time radiance field rendering. *ACM TOG*, 2023.

[28] Junho Kim, Changwoon Choi, Hojun Jang, and Young Min Kim. Piccolo: Point cloud-centric omnidirectional localization. In *CVPR*, 2021.

[29] Alex Krizhevsky, Ilya Sutskever, and Geoffrey E Hinton. Imagenet classification with deep convolutional neural networks. In *NeurIPS*, 2012.

[30] Shreyas Kulkarni, Peng Yin, and Sebastian Scherer. 360fusionnerf: Panoramic neural radiance fields with joint guidance. In *IROS*, 2023.

[31] Longwei Li, Huajian Huang, Sai-Kit Yeung, and Hui Cheng. Omnigs: Omnidirectional gaussian splatting for fast radiance field reconstruction using omnidirectional images. *arXiv preprint arXiv:2404.03202*, 2024.

[32] Ming Li, Xueqian Jin, Xuejiao Hu, Jingzhao Dai, Sidan Du, and Yang Li. Mode: Multi-view omnidirectional depth estimation with 360 cameras. In *ECCV*, 2022.

[33] Qiaoge Li, Itsuki Ueda, Chun Xie, Hidehiko Shishido, and Itaru Kitahara. Omnivoxel: A fast and precise reconstruction method of omnidirectional neural radiance field. In *GCCE*, 2022.

[34] Hidenobu Matsuki, Riku Murai, Paul HJ Kelly, and Andrew J Davison. Gaussian splatting slam. *arXiv preprint arXiv:2312.06741*, 2023.

[35] Andreas Meuleman, Hyeonjoong Jang, Daniel S Jeon, and Min H Kim. Real-time sphere sweeping stereo from multiview fisheye images. In *CVPR*, 2021.

[36] Ben Mildenhall, Pratul P. Srinivasan, Matthew Tancik, Jonathan T. Barron, Ravi Ramamoorthi, and Ren Ng. Nerf: Representing scenes as neural radiance fields for view synthesis. In *ECCV*, 2020.

[37] Pierre Moulon, Pascal Monasse, Romuald Perrot, and Renaud Marlet. OpenMVG: Open multiple view geometry. In *RRPR*, 2016.

[38] Alain Pagani and Didier Stricker. Structure from motion using full spherical panoramic cameras. In *ICCV Workshop*, 2011.

[39] Adam Paszke, Sam Gross, Francisco Massa, Adam Lerer, James Bradbury, Gregory Chanan, Trevor Killeen, Zeming Lin, Natalia Gimelshein, Luca Antiga, et al. PyTorch: An imperative style, high-performance deep learning library. In *NeurIPS*, 2019.

[40] Giovanni Pintore, Eva Almansa, Marco Agus, and Enrico Gobbetti. Deep3dlayout: 3d reconstruction of an indoor layout from a spherical panoramic image. *ACM TOG*, 2021.

[41] Shivansh Rao, Vikas Kumar, Daniel Kifer, C Lee Giles, and Ankur Mali. Omnilayout: Room layout reconstruction from indoor spherical panoramas. In *ICCV*, 2021.

[42] Davide Scaramuzza, Agostino Martinelli, and Roland Siegwart. A flexible technique for accurate omnidirectional camera calibration and structure from motion. In *ICVS*, 2006.

[43] Johannes L Schonberger and Jan-Michael Frahm. Structure-from-motion revisited. In *CVPR*, 2016.

[44] Shinya Sumikura, Mikiya Shibuya, and Ken Sakurada. Openvslam: A versatile visual slam framework. In *ACMMM*, 2019.

[45] Cheng Sun, Chi-Wei Hsiao, Ning-Hsu Wang, Min Sun, and Hwann-Tzong Chen. Indoor panorama planar 3d reconstruction via divide and conquer. In *ICCV*, 2021.

[46] Jiaxiang Tang, Jiawei Ren, Hang Zhou, Ziwei Liu, and Gang Zeng. Dreamgaussian: Generative gaussian splatting for efficient 3d content creation. In *ICLR*, 2024.

[47] Fu-En Wang, Yu-Hsuan Yeh, Min Sun, Wei-Chen Chiu, and Yi-Hsuan Tsai. Bifuse: Monocular 360 depth estimation via bi-projection fusion. In *CVPR*, 2020.

[48] Zhou Wang, Alan C Bovik, Hamid R Sheikh, Eero P Simoncelli, et al. Image quality assessment: From error visibility to structural similarity. *IEEE TIP*, 2004.

[49] Changhee Won, Hochang Seok, Zhaopeng Cui, Marc Pollefeys, and Jongwoo Lim. Omnislam: Omnidirectional localization and dense mapping for wide-baseline multi-camera systems. In *ICRA*, 2020.

[50] Guanjun Wu, Taoran Yi, Jiemin Fang, Lingxi Xie, Xiaopeng Zhang, Wei Wei, Wenyu Liu, Qi Tian, and Xinggang Wang. 4d gaussian splatting for real-time dynamic scene rendering. In *CVPR*, 2024.

[51] Qi Wu, Xiangyu Xu, Xieyuanli Chen, Ling Pei, Chao Long, Junyuan Deng, Guoqing Liu, Sheng Yang, Shilei Wen, and Wenxian Yu. 360-vio: A robust visual–inertial odometry using a 360° camera. *IEEE TIE*, 2023.

[52] Ziyi Yang, Xinyu Gao, Wen Zhou, Shaohui Jiao, Yuqing Zhang, and Xiaogang Jin. Deformable 3d gaussians for high-fidelity monocular dynamic scene reconstruction. In *CVPR*, 2023.

[53] Richard Zhang, Phillip Isola, Alexei A. Efros, Eli Shechtman, and Oliver Wang. The unreasonable effectiveness of deep features as a perceptual metric. In *CVPR*, 2018.

[54] Shijie Zhou, Zhiwen Fan, Dejia Xu, Haoran Chang, Pradyumna Chari, Tejas Bharadwaj, Suya You, Zhangyang Wang, and Achuta Kadambi. Dreamscene360: Unconstrained text-to-3d scene generation with panoramic gaussian splatting. In *ECCV*, 2024.

[55] Zehao Zhu, Zhiwen Fan, Yifan Jiang, and Zhangyang Wang. Fsgs: Real-time few-shot view synthesis using gaussian splatting. In *ECCV*, 2024.

[56] Matthias Zwicker, Hanspeter Pfister, Jeroen Van Baar, and Markus Gross. Ewa splatting. *IEEE TVCG*, 2002.

A Appendix / supplemental material

A.1 More Implementation Details

We follow the hyper-parameters of original 3DGS [27] excluding some hyperparameters. Firstly, we set *iterations* as 200k, *densify_until_iter* as 100k. However, we stopped the optimization after 100 minutes, regardless of the current iteration. For densification we set *percent_dense* as 1e-3, *densify_grad_threshold_min* (τ_{min}) as 2e-5, and *densify_grad_threshold_max* (τ_{max}) as 1e-4.

A.2 Proof of Mathematical Equivalence of the Derived Method

Here, we present the direct derivation of Eq. 8 by differentiating the omnidirectional projection function π_0 from Eq. 4.

$$
\begin{aligned}
\frac{\partial \pi_o(\boldsymbol{\mu})}{\partial \boldsymbol{\mu}} &= \begin{bmatrix} \frac{W}{2\pi}\frac{\boldsymbol{\mu}_z}{\boldsymbol{\mu}_x^2+\boldsymbol{\mu}_z^2} & 0 & -\frac{W}{2\pi}\frac{\boldsymbol{\mu}_x}{\boldsymbol{\mu}_x^2+\boldsymbol{\mu}_z^2} \\ -\frac{H}{\pi||\boldsymbol{\mu}||^2}\frac{\boldsymbol{\mu}_x\boldsymbol{\mu}_y}{\sqrt{\boldsymbol{\mu}_x^2+\boldsymbol{\mu}_z^2}} & \frac{H}{\pi||\boldsymbol{\mu}||^2}\sqrt{\boldsymbol{\mu}_x^2+\boldsymbol{\mu}_z^2} & -\frac{H}{\pi||\boldsymbol{\mu}||^2}\frac{\boldsymbol{\mu}_y\boldsymbol{\mu}_z}{\sqrt{\boldsymbol{\mu}_x^2+\boldsymbol{\mu}_z^2}} \end{bmatrix} \\
&= \begin{bmatrix} \frac{W}{2\pi||\boldsymbol{\mu}||}\frac{||\boldsymbol{\mu}||}{\sqrt{\boldsymbol{\mu}_x^2+\boldsymbol{\mu}_z^2}}\frac{\boldsymbol{\mu}_z}{\sqrt{\boldsymbol{\mu}_x^2+\boldsymbol{\mu}_z^2}} & 0 & -\frac{W}{2\pi||\boldsymbol{\mu}||}\frac{||\boldsymbol{\mu}||}{\sqrt{\boldsymbol{\mu}_x^2+\boldsymbol{\mu}_z^2}}\frac{\boldsymbol{\mu}_x}{\sqrt{\boldsymbol{\mu}_x^2+\boldsymbol{\mu}_z^2}} \\ \frac{H}{\pi||\boldsymbol{\mu}||}\frac{-\boldsymbol{\mu}_y}{||\boldsymbol{\mu}||}\frac{\boldsymbol{\mu}_x}{\sqrt{\boldsymbol{\mu}_x^2+\boldsymbol{\mu}_z^2}} & \frac{H}{\pi||\boldsymbol{\mu}||}\frac{\sqrt{\boldsymbol{\mu}_x^2+\boldsymbol{\mu}_z^2}}{||\boldsymbol{\mu}||} & \frac{H}{\pi||\boldsymbol{\mu}||}\frac{-\boldsymbol{\mu}_y}{||\boldsymbol{\mu}||}\frac{\boldsymbol{\mu}_z}{\sqrt{\boldsymbol{\mu}_x^2+\boldsymbol{\mu}_z^2}} \end{bmatrix} \\
&= \begin{bmatrix} \frac{W}{2\pi||\boldsymbol{\mu}||}\sec\theta_\mu\cos\phi_\mu & 0 & -\frac{W}{2\pi||\boldsymbol{\mu}||}\sec\theta_\mu\sin\phi_\mu \\ \frac{H}{\pi||\boldsymbol{\mu}||}\sin\theta_\mu\sin\phi_\mu & \frac{H}{\pi||\boldsymbol{\mu}||}\cos\theta_\mu & \frac{H}{\pi||\boldsymbol{\mu}||}\sin\theta_\mu\cos\phi_\mu \end{bmatrix} \\
&= \mathbf{J}_{omni}
\end{aligned} \tag{10}
$$

This proof demonstrates the mathematical correctness of our description outlined through Eq. 5, Eq. 6, and Eq. 7. The description in the main paper reveals the underlying assumptions (local affine approximation, tangent plane to sphere surface) and confirms their mathematical validity.

A.3 Back-Propagation of Rasterization in omnidirectional Image Domain

The gradient computation from Gaussian covariance is related to Eq. 10. We denote the gradient value matrix for the projected 2D covariance matrix(Σ) as $\frac{\partial L}{\partial \Sigma}$. The size of $\frac{\partial L}{\partial \Sigma}$ is 2×2, the same as the original covariance matrix. Note that the values of $\frac{\partial L}{\partial \Sigma}_{(1,2)}$ and $\frac{\partial L}{\partial \Sigma}_{(2,1)}$ are same since both Σ and $\frac{\partial L}{\partial \Sigma}$ are symmetric matrices.

We define $\mathbf{T}$ as $\mathbf{JW}$. The gradient value matrix of $\mathbf{T}$ is computed as below:

$$
\begin{aligned}
\frac{\partial \mathcal{L}}{\partial \mathbf{T}}_{(1,1)} &= 2\left(T_{(1,1)}V_{(1,1)} + T_{(1,2)}V_{(1,2)} + T_{(1,3)}V_{(1,3)}\right) * \frac{\partial \mathcal{L}}{\partial \mathbf{\Sigma}}_{(1,1)} \\
&\quad + \left(T_{(2,1)}V_{(1,1)} + T_{(2,2)}V_{(1,2)} + T_{(2,3)}V_{(1,3)}\right) * \frac{\partial \mathcal{L}}{\partial \mathbf{\Sigma}}_{(1,2)}, \\
\frac{\partial \mathcal{L}}{\partial \mathbf{T}}_{(1,2)} &= 2\left(T_{(1,1)}V_{(2,1)} + T_{(1,2)}V_{(2,2)} + T_{(1,3)}V_{(2,3)}\right) * \frac{\partial L}{\partial \mathbf{\Sigma}}_{(1,1)} \\
&\quad + \left(T_{(2,1)}V_{(2,1)} + T_{(2,2)}V_{(2,2)} + T_{(2,3)}V_{(2,3)}\right) * \frac{\partial L}{\partial \mathbf{\Sigma}}_{(1,2)}, \\
\frac{\partial \mathcal{L}}{\partial \mathbf{T}}_{(1,3)} &= 2\left(T_{(1,1)}V_{(3,1)} + T_{(1,2)}V_{(3,2)} + T_{(1,3)}V_{(3,3)}\right) * \frac{\partial L}{\partial \mathbf{\Sigma}}_{(1,1)} \\
&\quad + \left(T_{(2,1)}V_{(3,1)} + T_{(2,2)}V_{(3,2)} + T_{(2,3)}V_{(3,3)}\right) * \frac{\partial L}{\partial \mathbf{\Sigma}}_{(1,2)}, \\
\frac{\partial \mathcal{L}}{\partial \mathbf{T}}_{(2,1)} &= 2\left(T_{(2,1)}V_{(1,1)} + T_{(2,2)}V_{(1,2)} + T_{(2,3)}V_{(1,3)}\right) * \frac{\partial \mathcal{L}}{\partial \mathbf{\Sigma}}_{(2,2)} \\
&\quad + \left(T_{(1,1)}V_{(1,1)} + T_{(1,2)}V_{(1,2)} + T_{(1,3)}V_{(1,3)}\right) * \frac{\partial \mathcal{L}}{\partial \mathbf{\Sigma}}_{(1,2)}, \\
\frac{\partial \mathcal{L}}{\partial \mathbf{T}}_{(2,2)} &= 2\left(T_{(2,1)}V_{(2,1)} + T_{(2,2)}V_{(2,2)} + T_{(2,3)}V_{(2,3)}\right) * \frac{\partial \mathcal{L}}{\partial \mathbf{\Sigma}}_{(2,2)} \\
&\quad + \left(T_{(1,1)}V_{(2,1)} + T_{(1,2)}V_{(2,2)} + T_{(1,3)}V_{(2,3)}\right) * \frac{\partial \mathcal{L}}{\partial \mathbf{\Sigma}}_{(1,2)}, \\
\frac{\partial \mathcal{L}}{\partial \mathbf{T}}_{(2,3)} &= 2\left(T_{(2,1)}V_{(3,1)} + T_{(2,2)}V_{(3,2)} + T_{(2,3)}V_{(3,3)}\right) * \frac{\partial \mathcal{L}}{\partial \mathbf{\Sigma}}_{(2,2)} \\
&\quad + \left(T_{(1,1)}V_{(3,1)} + T_{(1,2)}V_{(3,2)} + T_{(1,3)}V_{(3,3)}\right) * \frac{\partial \mathcal{L}}{\partial \mathbf{\Sigma}}_{(1,2)}.
\end{aligned}
\tag{11}
$$

Then, the gradient for Jacobian matrix, $\frac{\partial \mathcal{L}}{\partial \mathbf{J}}$, is calculated as multiplication of $\mathbf{W}^T$ and $\frac{\partial \mathcal{L}}{\partial \mathbf{T}}$. After the gradient of $\mathbf{J}$ is calculated, the gradient for each position is computed as follows:

$$
\begin{aligned}
\frac{\partial \mathcal{L}}{\partial t_x} &= -\frac{W}{\pi} \cdot \frac{t_x t_z}{\left(t_x^2 + t_z^2\right)^2} \cdot \frac{\partial \mathcal{L}}{\partial \mathbf{J}}_{(1,1)} + \frac{W}{2\pi} \cdot \frac{t_x^2 - t_z^2}{\left(t_x^2 + t_z^2\right)^2} \cdot \frac{\partial \mathcal{L}}{\partial \mathbf{J}}_{(1,3)} \\
&\quad + \frac{H}{\pi} \cdot \frac{t_y\left(t_z^2 t_r^2 - 2t_x^2\left(t_x^2 + t_z^2\right)\right)}{t_r^4\left(t_x^2 + t_z^2\right)^{3/2}} \cdot \frac{\partial \mathcal{L}}{\partial \mathbf{J}}_{(2,1)} + \frac{H}{\pi} \cdot \frac{t_x\left(t_r^2 - 2t_y^2\right)}{t_r^4\sqrt{t_x^2 + t_z^2}} \cdot \frac{\partial \mathcal{L}}{\partial \mathbf{J}}_{(2,2)} \\
&\quad - \frac{H}{\pi} \cdot \frac{t_x t_y t_z\left(2\left(t_x^2 + t_z^2\right) + t_r^2\right)}{t_r^4\left(t_x^2 + t_z^2\right)^{3/2}} \cdot \frac{\partial \mathcal{L}}{\partial \mathbf{J}}_{(2,3)}. \\
\frac{\partial \mathcal{L}}{\partial t_y} &= +\frac{H}{\pi} \cdot \frac{t_x\left(t_r^2 - 2t_y^2\right)}{t_r^4\sqrt{t_x^2 + t_z^2}} \cdot \frac{\partial \mathcal{L}}{\partial \mathbf{J}}_{(2,1)} + \frac{2H}{\pi} \cdot \frac{t_y\sqrt{t_x^2 + t_z^2}}{t_r^4} \cdot \frac{\partial \mathcal{L}}{\partial \mathbf{J}}_{(2,2)} \\
&\quad + \frac{H}{\pi} \cdot \frac{t_z\left(t_r^2 - 2t_y^2\right)}{t_r^4\sqrt{t_x^2 + t_z^2}} \cdot \frac{\partial \mathcal{L}}{\partial \mathbf{J}}_{(2,3)}. \\
\frac{\partial \mathcal{L}}{\partial t_z} &= +\frac{W}{2\pi} \cdot \frac{t_x^2 - t_z^2}{\left(t_x^2 + t_z^2\right)^2} \cdot \frac{\partial \mathcal{L}}{\partial \mathbf{J}}_{(1,1)} + \frac{W}{\pi} \cdot \frac{t_x t_z}{\left(t_x^2 + t_z^2\right)^2} \cdot \frac{\partial \mathcal{L}}{\partial \mathbf{J}}_{(1,3)} \\
&\quad - \frac{H}{\pi} \cdot \frac{t_x t_y t_z\left(2\left(t_x^2 + t_z^2\right) + t_r^2\right)}{t_r^4\left(t_x^2 + t_z^2\right)^{3/2}} \cdot \frac{\partial \mathcal{L}}{\partial \mathbf{J}}_{(2,1)} + \frac{H}{\pi} \cdot \frac{t_z\left(t_r^2 - 2t_y^2\right)}{t_r^4\sqrt{t_x^2 + t_z^2}} \cdot \frac{\partial \mathcal{L}}{\partial \mathbf{J}}_{(2,2)} \\
&\quad + \frac{H}{\pi} \cdot \frac{t_y\left(t_x^2 t_r^2 - 2t_z^2\left(t_x^2 + t_z^2\right)\right)}{t_r^4\left(t_x^2 + t_z^2\right)^{3/2}} \cdot \frac{\partial \mathcal{L}}{\partial \mathbf{J}}_{(2,3)}.
\end{aligned}
\tag{12}
$$

A.4 Comparison with Original 3DGS with more input images.

Table A: Quantitative comparison of 3DGS (P) in 6-views and 18-views.

Dataset	Method	10 min PSNR↑	10 min SSIM↑	10 min LPIPS↓	100 min PSNR↑	100 min SSIM↑	100 min LPIPS↓
OmniBlender	3DGS (P6)	29.36	0.8770	0.1400	21.19	0.7528	0.3021
	3DGS (P18)	27.85	0.8387	0.1737	24.56	0.7907	0.2478
	ODGS	**32.76**	**0.9234**	**0.0469**	**33.05**	**0.9229**	**0.0343**
Ricoh360	3DGS (P6)	**25.12**	0.7932	0.2397	22.07	0.7228	0.3218
	3DGS (P18)	24.76	0.7726	0.2565	23.14	0.7277	0.3109
	ODGS	24.94	**0.8135**	**0.1489**	**26.27**	**0.8462**	**0.1051**
OmniPhotos	3DGS (P6)	25.61	0.8310	0.2100	23.30	0.7859	0.2670
	3DGS (P18)	24.93	0.8007	0.2412	23.21	0.7541	0.2996
	ODGS	**26.24**	**0.8704**	**0.1108**	**27.04**	**0.8878**	**0.0875**
360Roam	3DGS (P6)	20.17	0.7001	0.3536	19.34	0.6576	0.3837
	3DGS (P18)	20.88	0.6992	0.3571	**21.05**	0.6994	0.3405
	ODGS	**21.08**	**0.7066**	**0.3003**	20.85	**0.7111**	**0.2254**
OmniScenes	3DGS (P6)	23.61	0.8444	0.2835	17.14	0.7119	0.3906
	3DGS (P18)	24.00	0.8400	0.1993	21.43	0.7864	0.2828
	ODGS	**24.42**	**0.8526**	**0.1391**	**24.51**	**0.8505**	**0.1282**
360VO	3DGS (P6)	22.87	0.7861	0.2970	22.73	0.7822	0.3061
	3DGS (P18)	23.22	0.7875	0.2939	23.57	0.7938	0.2825
	ODGS	**24.63**	**0.8245**	**0.2175**	**26.68**	**0.8694**	**0.1264**

Although we report the results of the original 3DGS method using 6 cubemap decomposed perspective images in Table 1, we also compare the results when 3DGS is optimized with more perspective images. Whereas the original decomposition generates six perspective images for one omnidirectional image, the new decomposition produces 18 images by adding 12 perspective cameras where each camera faces an edge of the cube. Table A shows the performance of optimized results according to the number of perspective images for optimization. When using the 18 views (P18), the performance is comparable to the 6 views (P6) at the 10-minute mark but surpasses the 6 view results after the 100-minute optimization. At first, the increased number of images for training prevents the model from sufficiently learning from all views in the early stages (10 minutes), resulting in slightly lower performance. However, after sufficient optimization time (100 minutes) passes, the additional views allow for further optimization, leading to improved results. Still, ODGS shows the highest performance in most metrics, even considering 3DGS using 18 views, demonstrating the superiority of our rasterizer.

A.5 Detailed Quantitative Results

We provide detailed quantitative results that compose Table 1 below. We report PSNR, SSIM, and LPIPS of each method for all scenes in Table B - Table G. The tables show that our method outperforms all the baselines in almost all scenes. Please note that the *room1* scene in the OmniScenes dataset was omitted because the OpenMVG did not function properly due to the image sequence jumping in the middle. In Table 1, we report the averages of the scenes, excluding room1.

Table B: Quantitative comparison of 3D reconstruction results on Omniblender dataset (10min/100min). The best result for each metric is written in **bold**. Our method shows the best performance on almost all settings.

opt time	scene	Nerf(P)	3DGS(P)	TensoRF	EgoNeRF	ODGS
10min	archiviz-flat	20.42 / 0.7431 / 0.4028	31.20 / 0.9158 / 0.1044	28.44 / 0.8406 / 0.2751	29.06 / 0.8501 / 0.2477	**34.47 / 0.9499 / 0.0246**
	barbershop	19.50 / 0.6816 / 0.5540	33.25 / 0.9472 / 0.0849	27.58 / 0.8289 / 0.3259	31.13 / 0.9065 / 0.1793	**38.16 / 0.9778 / 0.0203**
	bistro bike	17.49 / 0.5145 / 0.6151	30.56 / 0.9298 / 0.0890	21.81 / 0.5978 / 0.4968	30.01 / 0.9065 / 0.1035	**33.87 / 0.9712 / 0.0195**
	bistro square	16.27 / 0.4960 / 0.6003	24.95 / 0.8887 / 0.1273	19.52 / 0.5620 / 0.4974	23.84 / 0.8298 / 0.1605	**28.59 / 0.9500 / 0.0269**
	classroom	18.16 / 0.6125 / 0.6144	26.89 / 0.8109 / 0.2291	25.02 / 0.7206 / 0.5100	26.33 / 0.7662 / 0.3740	**31.54 / 0.8674 / 0.1161**
	fisher hut	23.43 / 0.7171 / 0.4084	29.69 / 0.8153 / 0.1809	28.74 / 0.7549 / 0.4224	29.73 / 0.7780 / 0.3098	**32.39 / 0.8551 / 0.0610**
	lone monk	16.88 / 0.5561 / 0.5039	30.01 / 0.9204 / 0.1029	23.18 / 0.6933 / 0.3530	28.30 / 0.8777 / 0.1433	**33.49 / 0.9638 / 0.0201**
	LOU	17.79 / 0.6211 / 0.4705	30.68 / 0.9309 / 0.1030	27.60 / 0.8651 / 0.2174	30.89 / 0.9083 / 0.1171	**35.17 / 0.9573 / 0.0314**
	pavilion midday chair	19.99 / 0.7027 / 0.5128	29.69 / 0.9127 / 0.1015	26.33 / 0.7850 / 0.3237	29.01 / 0.8827 / 0.1354	**32.13 / 0.9499 / 0.0324**
	pavilion midday pond	17.86 / 0.5496 / 0.5690	24.82 / 0.7914 / 0.1797	22.11 / 0.6613 / 0.3091	23.86 / 0.7411 / 0.1963	**25.23 / 0.8125 / 0.0954**
	restroom	23.37 / 0.5421 / 0.6432	31.20 / 0.7840 / 0.2368	28.60 / 0.6644 / 0.5093	29.07 / 0.6930 / 0.4460	**35.37 / 0.9020 / 0.0684**
	average	19.20 / 0.6124 / 0.5359	29.36 / 0.8770 / 0.1400	25.36 / 0.7249 / 0.3855	28.29 / 0.8309 / 0.2194	**32.76 / 0.9234 / 0.0469**
100min	archiviz-flat	21.28 / 0.7326 / 0.3993	21.61 / 0.8054 / 0.2724	29.02 / 0.8504 / 0.2185	32.63 / 0.9175 / 0.1077	**34.10 / 0.9454 / 0.0243**
	barbershop	19.82 / 0.6584 / 0.5226	22.31 / 0.7708 / 0.3194	28.27 / 0.8479 / 0.2606	34.48 / 0.9551 / 0.0835	**37.89 / 0.9762 / 0.0204**
	bistro bike	18.12 / 0.5077 / 0.5828	19.39 / 0.7899 / 0.2414	22.58 / 0.6223 / 0.4310	33.23 / 0.9546 / 0.0471	**36.16 / 0.9752 / 0.0144**
	bistro square	17.06 / 0.5016 / 0.5616	21.27 / 0.8010 / 0.2414	19.86 / 0.5714 / 0.4319	25.49 / 0.8990 / 0.0940	**29.32 / 0.9536 / 0.0228**
	classroom	18.87 / 0.5968 / 0.5367	18.52 / 0.6499 / 0.4318	26.95 / 0.7481 / 0.4384	29.55 / 0.8306 / 0.2652	**31.54 / 0.8524 / 0.0567**
	fisher hut	24.87 / 0.7221 / 0.3964	25.92 / 0.7872 / 0.2380	28.74 / 0.7514 / 0.3566	30.32 / 0.8018 / 0.2338	**32.75 / 0.8604 / 0.0525**
	lone monk	17.27 / 0.5459 / 0.4828	19.12 / 0.7479 / 0.3114	23.73 / 0.7161 / 0.2889	30.90 / 0.9311 / 0.0800	**32.88 / 0.9608 / 0.0180**
	LOU	19.93 / 0.6619 / 0.4103	21.59 / 0.8199 / 0.2515	28.60 / 0.8430 / 0.1756	33.53 / 0.9400 / 0.0693	**35.43 / 0.9573 / 0.0277**
	pavilion midday chair	21.38 / 0.6994 / 0.4329	19.62 / 0.7522 / 0.3360	27.11 / 0.8015 / 0.2558	31.08 / 0.9315 / 0.0648	**32.93 / 0.9562 / 0.0266**
	pavilion midday pond	17.60 / 0.5346 / 0.5142	20.89 / 0.7267 / 0.2596	22.59 / 0.6795 / 0.2512	25.71 / 0.8145 / 0.1240	**25.40 / 0.8189 / 0.0783**
	restroom	24.20 / 0.5407 / 0.6039	22.91 / 0.6301 / 0.4204	29.49 / 0.7261 / 0.3787	32.86 / 0.8515 / 0.2167	**35.14 / 0.8957 / 0.0354**
	average	20.04 / 0.6092 / 0.4949	21.19 / 0.7528 / 0.3021	26.08 / 0.7416 / 0.3170	30.89 / 0.8934 / 0.1260	**33.05 / 0.9229 / 0.0343**

Table C: Quantitative comparison of 3D reconstruction results on Ricoh360 dataset (10min/100min). The best result for each metric is written in **bold**. Our method shows the best performance on almost all settings.

opt. time	scene	NeRF(P)	3DGS(P)	TensoRF	EgoNeRF	ODGS
10min	bricks	12.40 / 0.4489 / 0.6403	23.88 / 0.7875 / 0.2275	21.08 / 0.6201 / 0.4918	23.09 / 0.7223 / 0.2984	**23.90/ 0.8185 / 0.1296**
	bridge	14.96 / 0.5553 / 0.5866	23.78 / 0.7783 / 0.2145	21.93 / 0.6456 / 0.4823	23.34 / 0.7199 / 0.3096	**23.88 / 0.7987 / 0.1286**
	bridge under	19.71 / 0.4987 / 0.6769	24.30 / 0.7892 / 0.2239	21.99 / 0.6323 / 0.5791	24.11 / 0.7504 / 0.3202	**25.12 / 0.8347 / 0.1339**
	cat tower	12.54 / 0.5182 / 0.5990	24.33 / 0.7543 / 0.2548	22.45 / 0.6308 / 0.6002	23.80 / 0.6861 / 0.3758	**24.47 / 0.7771 / 0.1435**
	center	14.76 / 0.6691 / 0.5211	27.24 / 0.8364 / 0.2887	27.23 / 0.8088 / 0.4294	27.97 / 0.8450 / 0.2521	**28.10 / 0.8710 / 0.1206**
	farm	14.45 / 0.4970 / 0.6262	21.66 / **0.6897** / 0.3248	20.80 / 0.5683 / 0.5141	**21.80** / 0.6483 / 0.3386	20.74 / 0.6881 / **0.2270**
	flower	12.03 / 0.4132 / 0.6912	21.71 / 0.6942 / 0.3247	20.07 / 0.5414 / 0.6696	21.51 / 0.6149 / 0.4211	**22.19 / 0.7273 / 0.1925**
	gallery chair	15.40 / 0.6950 / 0.4929	**27.76** / 0.8732 / 0.1962	26.00 / 0.7907 / 0.5233	27.01 / 0.8326 / 0.3409	27.29 / **0.8777 / 0.1353**
	gallery park	12.29 / 0.6050 / 0.5176	25.30 / 0.8021 / 0.2384	24.21 / 0.7394 / 0.5120	25.11 / 0.7703 / 0.3245	**25.48 / 0.8241 / 0.1341**
	gallery pillar	14.50 / 0.6445 / 0.4902	27.79 / 0.8613 / 0.1617	25.85 / 0.7821 / 0.3977	27.31 / 0.8312 / 0.2379	**28.02 / 0.8821 / 0.0882**
	garden	13.97 / 0.5682 / 0.5430	**27.53 / 0.7919 / 0.2118**	25.37 / 0.6649 / 0.5616	26.48 / 0.7175 / 0.3517	23.20 / 0.7843 / 0.2289
	poster	14.99 / 0.6258 / 0.5679	26.14 / 0.8599 / 0.2098	23.20 / 0.7500 / 0.4784	25.39 / 0.8213 / 0.3205	**26.90 / 0.8782 / 0.1249**
	average	14.33 / 0.5616 / 0.5794	**25.12** / 0.7932 / 0.2397	23.35 / 0.6812 / 0.5200	24.74 / 0.7467 / 0.3243	24.94 / **0.8135 / 0.1489**
100min	bricks	15.01 / 0.4760 / 0.6245	22.60 / 0.7410 / 0.2855	21.66 / 0.6353 / 0.4375	23.93 / 0.7616 / 0.2475	**24.62 / 0.8479 / 0.1021**
	bridge	17.32 / 0.5558 / 0.5620	21.94 / 0.7157 / 0.3133	22.58 / 0.6558 / 0.4306	23.94 / 0.7516 / 0.2562	**24.37 / 0.8154 / 0.1063**
	bridge under	16.42 / 0.5075 / 0.6447	19.03 / 0.6377 / 0.3663	22.86 / 0.6577 / 0.4826	25.05 / 0.7924 / 0.2492	**25.93 / 0.8538 / 0.1026**
	cat tower	15.45 / 0.5323 / 0.5824	21.24 / 0.6851 / 0.3565	23.02 / 0.6393 / 0.5477	24.52 / 0.7163 / 0.3417	**25.35 / 0.8088 / 0.1109**
	center	17.09 / 0.6566 / 0.4955	20.04 / 0.6974 / 0.4237	27.90 / 0.8182 / 0.3840	29.12 / 0.8625 / 0.2119	**29.39 / 0.8940 / 0.0808**
	farm	15.93 / 0.4830 / 0.6173	21.49 / **0.6844** / 0.3299	21.09 / 0.5765 / 0.4662	**22.25** / 0.6745 / **0.3089**	16.34 / 0.6039 / 0.4109
	flower	13.57 / 0.4153 / 0.6845	20.48 / 0.6559 / 0.3531	20.57 / 0.5506 / 0.6161	22.08 / 0.6497 / 0.3922	**22.71 / 0.7485 / 0.1509**
	gallery chair	17.59 / 0.6873 / 0.5240	26.44 / 0.8509 / 0.2161	26.61 / 0.7990 / 0.4766	**27.71** / 0.8505 / 0.2993	27.62 / **0.8831 / 0.1135**
	gallery park	14.24 / 0.5847 / 0.5404	23.22 / 0.7637 / 0.3027	24.64 / 0.7457 / 0.4724	25.64 / 0.7848 / 0.3001	**26.19 / 0.8401 / 0.1076**
	gallery pillar	16.57 / 0.6405 / 0.4946	21.93 / 0.7429 / 0.3205	26.49 / 0.7960 / 0.3336	27.97 / 0.8467 / 0.2104	**28.74 / 0.8970 / 0.0693**
	garden	17.81 / 0.5840 / 0.5101	25.97 / 0.7792 / 0.2528	25.91 / 0.6738 / 0.5201	**27.16** / 0.7441 / 0.3112	27.09 / **0.8383 / 0.1006**
	poster	16.91 / 0.6169 / 0.5794	20.45 / 0.7199 / 0.3406	24.32 / 0.7750 / 0.4161	26.50 / 0.8497 / 0.2613	**26.92 / 0.8808 / 0.1113**
	average	16.16 / 0.5617 / 0.5716	22.07 / 0.7228 / 0.3218	23.97 / 0.6936 / 0.4653	**25.49** / 0.7737 / 0.2825	25.44 / **0.8260 / 0.1306**

Table D: Quantitative comparison of 3D reconstruction results on Omniphotos dataset (10min/100min). The best result for each metric is written in **bold**. Our method shows the best performance on almost all settings.

opt time	scene	Nerf(P)	3DGS(P)	TensoRF	EgoNeRF	ODGS
10min	Ballintoy	19.90 / 0.7292 / 0.4717	28.67 / 0.8875 / 0.2094	25.68 / 0.8008 / 0.4190	28.49 / 0.8715 / 0.2270	**29.11** / **0.9085** / **0.1076**
	BeihaiPark	16.76 / 0.5946 / 0.5871	23.39 / 0.8126 / 0.2600	22.16 / 0.6855 / 0.5516	24.35 / 0.7755 / 0.2682	**25.34** / **0.8600** / **0.1409**
	Cathedral	15.38 / 0.4736 / 0.6851	23.01 / 0.7885 / 0.2569	19.35 / 0.5638 / 0.5511	23.11 / 0.7267 / 0.2898	**23.74** / **0.8394** / **0.1416**
	Coast	20.38 / 0.6452 / 0.5253	27.86 / 0.8378 / 0.2011	24.69 / 0.7026 / 0.4440	27.74 / 0.8006 / 0.2320	**28.75** / **0.8837** / **0.0966**
	Field	23.44 / 0.7063 / 0.4293	29.51 / 0.8392 / 0.1600	27.25 / 0.7427 / 0.4602	28.53 / 0.7843 / 0.2618	**29.71** / **0.8702** / **0.0892**
	Nunobiki2	18.79 / 0.6182 / 0.5295	**24.84** / 0.8017 / 0.2224	22.93 / 0.6719 / 0.5308	23.45 / 0.7052 / 0.3378	21.62 / **0.8289** / **0.1496**
	SecretGarden1	17.96 / 0.6380 / 0.5040	25.48 / 0.8579 / 0.1706	22.49 / 0.7065 / 0.5205	24.87 / 0.7885 / 0.2450	**27.53** / **0.8940** / **0.0769**
	Shrines1	15.67 / 0.4516 / 0.7258	22.36 / 0.7449 / 0.2864	19.52 / 0.5179 / 0.6441	21.28 / 0.6374 / 0.3693	**23.45** / **0.8108** / **0.1560**
	Temple3	15.27 / 0.5932 / 0.6112	25.17 / 0.8549 / 0.1839	20.83 / 0.6800 / 0.5691	24.31 / 0.7916 / 0.2321	**26.14** / **0.8881** / **0.0868**
	Wulongting	17.89 / 0.7083 / 0.4451	25.80 / 0.8845 / 0.1497	22.89 / 0.7697 / 0.3987	25.89 / 0.8405 / 0.1991	**26.98** / **0.9203** / **0.0626**
	average	18.14 / 0.6158 / 0.5514	25.61 / 0.8310 / 0.2100	22.78 / 0.6841 / 0.5089	25.20 / 0.7722 / 0.2662	**26.24** / **0.8704** / **0.1108**
100min	Ballintoy	23.32 / 0.7538 / 0.3796	26.37 / 0.8694 / 0.2286	26.85 / 0.8193 / 0.3738	29.83 / 0.8981 / 0.1827	**30.06** / **0.9220** / **0.0780**
	BeihaiPark	18.48 / 0.6089 / 0.4949	20.81 / 0.7581 / 0.2898	23.13 / 0.7095 / 0.4783	**26.19** / **0.8390** / **0.1778**	19.94 / 0.7955 / 0.2352
	Cathedral	18.01 / 0.5032 / 0.6033	20.18 / 0.6879 / 0.3682	20.23 / 0.5935 / 0.4848	24.88 / 0.8056 / 0.1878	**25.39** / **0.8769** / **0.1081**
	Coast	23.12 / 0.6666 / 0.4263	27.29 / 0.8334 / 0.2091	26.27 / 0.7329 / 0.3868	**29.28** / 0.8553 / 0.1627	29.23 / **0.9004** / **0.0770**
	Field	25.81 / 0.7274 / 0.3980	29.36 / 0.8420 / 0.1665	27.72 / 0.7488 / 0.4209	**30.04** / 0.8374 / 0.1776	29.18 / **0.8866** / **0.0851**
	Nunobiki2	21.02 / 0.6346 / 0.4705	20.30 / 0.7116 / 0.3662	23.63 / 0.6866 / 0.4686	25.13 / 0.7879 / 0.2115	**25.78** / **0.8659** / **0.0996**
	SecretGarden1	20.46 / 0.6573 / 0.4641	23.93 / 0.8470 / 0.2015	23.39 / 0.7273 / 0.4548	26.76 / 0.8514 / 0.1513	**27.54** / **0.8963** / **0.0725**
	Shrines1	18.13 / 0.4803 / 0.6417	21.32 / 0.7266 / 0.2910	20.01 / 0.5285 / 0.5717	22.83 / 0.7313 / 0.2495	**23.94** / **0.8270** / **0.1319**
	Temple3	18.69 / 0.6232 / 0.5202	22.22 / 0.7889 / 0.2523	22.06 / 0.7041 / 0.4840	**26.21** / 0.8518 / 0.1411	24.58 / **0.8895** / **0.0822**
	Wulongting	20.98 / 0.7328 / 0.3736	21.23 / 0.7945 / 0.2964	24.02 / 0.7875 / 0.3434	**27.84** / 0.8914 / 0.1240	27.66 / **0.9255** / **0.0531**
	average	20.80 / 0.6388 / 0.4772	23.30 / 0.7859 / 0.2670	23.73 / 0.7038 / 0.4467	**26.90** / 0.8349 / 0.1766	26.33 / **0.8786** / **0.1023**

Table E: Quantitative comparison of 3D reconstruction results on 360Roam dataset (10min/100min). The best result for each metric is written in **bold**. Our method shows the best performance on almost all settings.

opt time	scene	Nerf(P)	3DGS(P)	TensoRF	EgoNeRF	ODGS
10min	bar	13.49 / 0.6218 / 0.5246	18.75 / **0.6982** / 0.3347	15.98 / 0.5212 / 0.7717	18.34 / 0.5713 / 0.4191	**19.25** / 0.6892 / **0.3078**
	base	14.18 / 0.6530 / 0.5849	20.55 / **0.6965** / 0.3086	17.34 / 0.5358 / 0.8291	19.44 / 0.5808 / 0.5852	**20.93** / 0.6777 / **0.3044**
	cafe	14.60 / 0.6645 / 0.4988	**20.35** / **0.7503** / **0.2685**	17.15 / 0.5462 / 0.7526	19.04 / 0.6515 / 0.4789	20.23 / 0.7424 / 0.2699
	canteen	14.00 / 0.6885 / 0.5026	18.83 / **0.6716** / 0.3801	17.36 / 0.5841 / 0.7301	17.60 / 0.5892 / 0.5989	**19.13** / 0.6658 / **0.3622**
	center	15.96 / 0.7035 / 0.4507	20.66 / 0.7020 / 0.3799	18.11 / 0.6290 / 0.7740	21.46 / 0.6756 / 0.5736	**22.40** / **0.7477** / **0.3135**
	center1	15.77 / **0.7330** / 0.4300	18.70 / 0.7082 / 0.4186	18.52 / 0.6697 / 0.7354	21.56 / 0.6930 / 0.5805	**22.15** / 0.7221 / **0.3260**
	corridor	16.32 / **0.7468** / 0.4231	21.07 / 0.7329 / 0.3289	18.70 / 0.6680 / 0.6500	21.12 / 0.6764 / 0.5130	**21.73** / 0.7335 / **0.2666**
	innovation	14.47 / 0.6423 / 0.5076	21.07 / **0.6902** / 0.3302	18.84 / 0.5711 / 0.7583	20.72 / 0.6279 / 0.4997	**21.54** / 0.6824 / **0.3212**
	lab	15.33 / 0.7626 / 0.4248	22.77 / 0.8098 / 0.2268	18.92 / 0.6622 / 0.6989	20.54 / 0.7110 / 0.4526	**23.15** / **0.8172** / **0.1566**
	library	16.01 / 0.6325 / 0.5107	**22.71** / **0.6480** / 0.3662	18.02 / 0.5884 / 0.7884	21.39 / 0.5926 / 0.6001	22.46 / 0.6435 / **0.2964**
	office	15.64 / 0.6847 / 0.4650	16.47 / 0.5937 / 0.5469	19.04 / 0.6108 / 0.7479	**21.62** / 0.6246 / 0.5658	18.94 / **0.6516** / **0.3787**
	average	15.07 / 0.6848 / 0.4839	20.17 / 0.7001 / 0.3536	18.00 / 0.5988 / 0.7488	20.45 / 0.6358 / 0.5334	**21.08** / **0.7066** / **0.3003**
100min	bar	14.12 / 0.6370 / 0.5174	18.64 / 0.6633 / 0.3487	16.06 / 0.5196 / 0.7395	19.35 / 0.6362 / 0.3194	**19.68** / **0.7152** / **0.2250**
	base	14.73 / 0.6634 / 0.5930	20.83 / 0.7057 / 0.2756	17.40 / 0.5158 / 0.7792	20.05 / 0.6214 / 0.4797	**21.33** / **0.7098** / **0.1945**
	cafe	14.96 / 0.6666 / 0.5169	19.03 / 0.6672 / 0.3333	17.30 / 0.5397 / 0.7127	19.56 / 0.6912 / 0.3876	**20.43** / **0.7641** / **0.1783**
	canteen	14.20 / 0.6761 / 0.5206	17.51 / 0.6100 / 0.4184	17.47 / 0.5799 / 0.7118	18.36 / 0.6192 / 0.5251	**19.06** / **0.6661** / **0.2733**
	center	15.70 / 0.6982 / 0.4644	20.79 / 0.6847 / 0.3846	18.22 / 0.6217 / 0.7426	22.09 / 0.6991 / 0.4954	**22.79** / **0.7629** / **0.2094**
	center1	15.27 / **0.7203** / 0.4557	19.91 / 0.7017 / 0.3990	18.57 / 0.6629 / 0.7072	**22.17** / 0.7152 / 0.5039	18.36 / 0.6531 / **0.3337**
	corridor	16.21 / 0.7333 / 0.4537	18.47 / 0.6596 / 0.4131	19.10 / 0.6638 / 0.6212	21.07 / 0.6912 / 0.4632	**21.96** / **0.7337** / **0.2106**
	innovation	14.86 / 0.6412 / 0.5162	20.56 / 0.6552 / 0.3483	19.06 / 0.5671 / 0.7170	21.71 / 0.6778 / 0.3931	**21.93** / **0.7131** / **0.2089**
	lab	15.87 / 0.7538 / 0.4560	20.79 / 0.7280 / 0.3166	19.14 / 0.6589 / 0.6508	22.14 / 0.7600 / 0.3263	**23.39** / **0.8258** / **0.1139**
	library	16.06 / 0.6258 / 0.5453	19.95 / 0.5715 / 0.4528	17.77 / 0.5495 / 0.7623	**22.39** / 0.6295 / 0.4988	22.02 / **0.6341** / **0.2209**
	office	15.93 / **0.6783** / 0.4888	16.22 / 0.5867 / 0.5304	19.29 / 0.6059 / 0.7021	**22.23** / 0.6485 / 0.4960	18.44 / 0.6439 / **0.3109**
	average	15.26 / 0.6813 / 0.5025	19.34 / 0.6576 / 0.3837	18.12 / 0.5895 / 0.7133	**21.18** / 0.6718 / 0.4444	20.85 / **0.7111** / **0.2254**

Table F: Quantitative comparison of 3D reconstruction results on OmniScenes dataset (10min/100min). The best result for each metric is written in **bold**. Our method shows the best performance on almost all settings.

opt time	scene	Nerf(P)	3DGS(P)	TensoRF	EgoNeRF	ODGS
10min	pyebaekRoom 1	14.76 / 0.5940 / 0.5417	20.56 / 0.7347 / 0.2525	21.69 / 0.6800 / 0.4751	21.13 / 0.7055 / 0.3934	**22.78** / **0.8038** / **0.1449**
	room 1	15.14 / 0.7264 / 0.4518	22.48 / 0.8566 / 0.1985	19.81 / 0.8159 / 0.3020	21.68 / 0.7908 / 0.3358	- / - / -
	room 2	15.09 / 0.7156 / 0.4563	22.90 / 0.8277 / 0.1979	23.24 / 0.8042 / 0.3425	22.51 / 0.7837 / 0.3411	**24.17** / **0.8303** / **0.1302**
	room 3	16.21 / 0.7811 / 0.3790	25.13 / **0.8860** / 0.1554	**26.39** / 0.8708 / 0.3022	22.79 / 0.8423 / 0.3454	24.08 / 0.8743 / **0.1384**
	room 4	15.52 / 0.7467 / 0.4202	25.61 / 0.8816 / 0.1656	24.97 / 0.8583 / 0.2901	24.66 / 0.8434 / 0.3117	**26.14** / **0.8906** / **0.1052**
	room 5	16.75 / 0.8105 / 0.3805	24.43 / **0.8915** / 0.1843	**25.52** / 0.8855 / 0.3198	22.87 / 0.8583 / 0.3416	24.49 / 0.8819 / **0.1493**
	weddingHall 1	16.40 / 0.6783 / 0.5529	24.18 / 0.8326 / 0.8304	23.42 / 0.7680 / 0.4419	23.85 / 0.7741 / 0.3552	**24.83** / **0.8347** / **0.1664**
	average	15.79 / 0.7210 / 0.4551	23.80 / 0.8424 / 0.2977	24.21 / 0.8111 / 0.3619	22.97 / 0.8012 / 0.3481	**24.42** / **0.8526** / **0.1391**
100min	pyebaekRoom 1	15.99 / 0.5932 / 0.5669	17.71 / 0.6282 / 0.4094	22.57 / 0.6993 / 0.4026	**23.69** / 0.7688 / 0.2787	22.91 / **0.8068** / **0.1322**
	room 1	14.64 / 0.6604 / 0.4850	11.49 / 0.5864 / 0.5746	19.99 / 0.8226 / 0.2797	22.44 / 0.8083 / 0.2715	- / - / -
	room 2	14.66 / 0.6464 / 0.5138	11.68 / 0.6005 / 0.5027	23.58 / 0.8083 / 0.3037	**23.53** / 0.8086 / 0.2786	23.13 / **0.8108** / **0.1422**
	room 3	16.37 / 0.7657 / 0.4280	20.13 / 0.8066 / 0.3109	**27.26** / 0.8793 / 0.2631	26.43 / 0.8789 / 0.2364	25.56 / **0.8847** / **0.1150**
	room 4	16.13 / 0.7182 / 0.4724	19.18 / 0.7712 / 0.3390	26.06 / 0.8682 / 0.2495	26.17 / 0.8693 / 0.2336	**26.25** / **0.8879** / **0.1025**
	room 5	17.43 / 0.7996 / 0.4195	17.93 / 0.8088 / 0.3336	26.01 / **0.8894** / 0.2834	**26.06** / 0.8803 / 0.2652	24.44 / 0.8797 / **0.1383**
	weddingHall 1	16.64 / 0.6398 / 0.5541	21.85 / 0.7818 / 0.2642	24.04 / 0.7786 / 0.3818	**25.00** / 0.8052 / 0.2718	24.77 / **0.8331** / **0.1392**
	average	16.20 / 0.6838 / 0.4925	18.08 / 0.7329 / 0.3600	24.92 / 0.8205 / 0.3140	**25.15** / 0.8352 / 0.2607	24.51 / **0.8505** / **0.1282**

Table G: Quantitative comparison of 3D reconstruction results on 360VO dataset (10min/100min). The best result for each metric is written in **bold**. Our method shows the best performance on almost all settings.

opt time	scene	Nerf(P)	3DGS(P)	TensoRF	EgoNeRF	ODGS
10min	seq0	15.72 / 0.6574 / 0.4639	17.70 / 0.7101 / 0.3946	19.61 / 0.6975 / 0.5622	**21.46** / 0.7229 / 0.4575	20.99 / **0.7750** / **0.2983**
	seq1	15.58 / 0.5683 / 0.5255	24.31 / 0.7986 / 0.2639	20.59 / 0.6448 / 0.6457	23.33 / 0.6976 / 0.4372	**26.42** / **0.8297** / **0.2069**
	seq2	18.04 / 0.5774 / 0.5304	30.44 / 0.9055 / 0.1283	23.69 / 0.6830 / 0.5402	27.46 / 0.7945 / 0.3068	**31.61** / **0.9195** / **0.0779**
	seq3	15.81 / 0.5165 / 0.5740	20.50 / 0.6455 / 0.4518	20.53 / 0.5789 / 0.6819	20.10 / 0.5768 / 0.5903	**21.72** / **0.6997** / **0.3430**
	seq4	14.97 / 0.5853 / 0.5469	27.81 / 0.8646 / 0.1686	21.73 / 0.6673 / 0.5616	24.51 / 0.7395 / 0.3755	**28.31** / **0.8917** / **0.1116**
	seq5	15.97 / 0.6765 / 0.4242	19.20 / 0.7601 / 0.3380	19.68 / 0.7295 / 0.4952	21.18 / 0.7595 / 0.3971	**21.69** / **0.8487** / **0.2034**
	seq6	15.49 / 0.5380 / 0.5104	**26.01** / **0.8018** / **0.2436**	19.61 / 0.5996 / 0.5842	21.83 / 0.6470 / 0.4595	25.10 / 0.7858 / 0.2518
	seq7	15.46 / 0.6421 / 0.5045	25.42 / 0.8273 / 0.2419	11.13 / 0.5474 / 0.7262	22.72 / 0.7224 / 0.4725	**26.36** / **0.8388** / **0.2210**
	seq8	14.67 / 0.6730 / 0.4519	21.31 / 0.7900 / 0.3202	21.10 / 0.7409 / 0.4910	**23.94** / 0.7814 / 0.3694	23.09 / **0.8316** / **0.2439**
	seq9	15.43 / 0.7510 / 0.4168	15.98 / 0.7572 / 0.4194	20.69 / 0.7976 / 0.5313	19.65 / 0.7823 / 0.4803	**21.04** / **0.8373** / **0.2972**
	average	15.71 / 0.6186 / 0.4949	22.87 / 0.7861 / 0.2970	19.74 / 0.6543 / 0.5876	22.62 / 0.7224 / 0.4346	**24.63** / **0.8245** / **0.2175**
100min	seq0	17.16 / 0.6623 / 0.4865	18.31 / 0.7185 / 0.3880	19.92 / 0.6959 / 0.5528	**22.25** / 0.7466 / 0.4081	21.69 / **0.8062** / **0.2214**
	seq1	17.16 / 0.5843 / 0.5439	24.59 / 0.8081 / 0.2451	21.06 / 0.6505 / 0.6221	24.43 / 0.7352 / 0.3685	**28.40** / **0.8777** / **0.0961**
	seq2	19.25 / 0.5867 / 0.5350	29.99 / 0.9014 / 0.1298	24.44 / 0.7032 / 0.4944	29.22 / 0.8492 / 0.2230	**30.58** / **0.9187** / **0.0644**
	seq3	18.01 / 0.5398 / 0.5867	20.67 / 0.6464 / 0.4394	21.16 / 0.5850 / 0.6533	21.01 / 0.6101 / 0.5366	**22.59** / **0.7632** / **0.2271**
	seq4	17.27 / 0.6053 / 0.5461	25.64 / 0.8336 / 0.2285	22.40 / 0.6769 / 0.5307	26.46 / 0.7949 / 0.2737	**30.20** / **0.9298** / **0.0564**
	seq5	17.31 / 0.6816 / 0.4423	19.74 / 0.7682 / 0.3367	19.95 / 0.7239 / 0.4945	22.19 / 0.7867 / 0.3422	**22.86** / **0.8778** / **0.1398**
	seq6	17.88 / 0.5691 / 0.5072	26.36 / 0.8063 / 0.2475	20.26 / 0.6086 / 0.5664	23.93 / 0.7021 / 0.3775	**29.07** / **0.8982** / **0.0807**
	seq7	17.94 / 0.6729 / 0.5099	24.90 / 0.8025 / 0.2896	11.01 / 0.5349 / 0.7288	24.43 / 0.7599 / 0.3903	**28.07** / **0.8833** / **0.1252**
	seq8	17.61 / 0.6948 / 0.4818	21.15 / 0.7761 / 0.3391	21.72 / 0.7435 / 0.4811	**25.29** / 0.8126 / 0.3132	24.01 / **0.8673** / **0.1800**
	seq9	18.23 / 0.7764 / 0.4250	15.94 / 0.7610 / 0.4177	21.19 / 0.7981 / 0.5162	19.90 / 0.7935 / 0.4463	**20.09** / **0.8290** / **0.2725**
	average	17.78 / 0.6373 / 0.5064	22.73 / 0.7822 / 0.3061	20.50 / 0.6885 / 0.5531	23.91 / 0.7591 / 0.3679	**26.68** / **0.8694** / **0.1264**

NeurIPS Paper Checklist

The checklist is designed to encourage best practices for responsible machine learning research, addressing issues of reproducibility, transparency, research ethics, and societal impact. Do not remove the checklist: **The papers not including the checklist will be desk rejected.** The checklist should follow the references and precede the (optional) supplemental material. The checklist does NOT count towards the page limit.

Please read the checklist guidelines carefully for information on how to answer these questions. For each question in the checklist:

- You should answer [Yes] , [No] , or [NA] .
- [NA] means either that the question is Not Applicable for that particular paper or the relevant information is Not Available.
- Please provide a short (1–2 sentence) justification right after your answer (even for NA).

The checklist answers are an integral part of your paper submission. They are visible to the reviewers, area chairs, senior area chairs, and ethics reviewers. You will be asked to also include it (after eventual revisions) with the final version of your paper, and its final version will be published with the paper.

The reviewers of your paper will be asked to use the checklist as one of the factors in their evaluation. While "[Yes] " is generally preferable to "[No] ", it is perfectly acceptable to answer "[No] " provided a proper justification is given (e.g., "error bars are not reported because it would be too computationally expensive" or "we were unable to find the license for the dataset we used"). In general, answering "[No] " or "[NA] " is not grounds for rejection. While the questions are phrased in a binary way, we acknowledge that the true answer is often more nuanced, so please just use your best judgment and write a justification to elaborate. All supporting evidence can appear either in the main paper or the supplemental material, provided in appendix. If you answer [Yes] to a question, in the justification please point to the section(s) where related material for the question can be found.

IMPORTANT, please:

- **Delete this instruction block, but keep the section heading "NeurIPS paper checklist"**,
- **Keep the checklist subsection headings, questions/answers and guidelines below.**
- **Do not modify the questions and only use the provided macros for your answers**.

1. **Claims**

   Question: Do the main claims made in the abstract and introduction accurately reflect the paper's contributions and scope?

   Answer: [Yes]

   Justification: The abstract and introduction explain the motivation and the core idea of our work.

   Guidelines:

   - The answer NA means that the abstract and introduction do not include the claims made in the paper.
   - The abstract and/or introduction should clearly state the claims made, including the contributions made in the paper and important assumptions and limitations. A No or NA answer to this question will not be perceived well by the reviewers.
   - The claims made should match theoretical and experimental results, and reflect how much the results can be expected to generalize to other settings.
   - It is fine to include aspirational goals as motivation as long as it is clear that these goals are not attained by the paper.

2. **Limitations**

   Question: Does the paper discuss the limitations of the work performed by the authors?

   Answer: [Yes]

Justification: We wrote the limitation and the topics for future works in the subsection of conclusion.

Guidelines:

- The answer NA means that the paper has no limitation while the answer No means that the paper has limitations, but those are not discussed in the paper.
- The authors are encouraged to create a separate "Limitations" section in their paper.
- The paper should point out any strong assumptions and how robust the results are to violations of these assumptions (e.g., independence assumptions, noiseless settings, model well-specification, asymptotic approximations only holding locally). The authors should reflect on how these assumptions might be violated in practice and what the implications would be.
- The authors should reflect on the scope of the claims made, e.g., if the approach was only tested on a few datasets or with a few runs. In general, empirical results often depend on implicit assumptions, which should be articulated.
- The authors should reflect on the factors that influence the performance of the approach. For example, a facial recognition algorithm may perform poorly when image resolution is low or images are taken in low lighting. Or a speech-to-text system might not be used reliably to provide closed captions for online lectures because it fails to handle technical jargon.
- The authors should discuss the computational efficiency of the proposed algorithms and how they scale with dataset size.
- If applicable, the authors should discuss possible limitations of their approach to address problems of privacy and fairness.
- While the authors might fear that complete honesty about limitations might be used by reviewers as grounds for rejection, a worse outcome might be that reviewers discover limitations that aren't acknowledged in the paper. The authors should use their best judgment and recognize that individual actions in favor of transparency play an important role in developing norms that preserve the integrity of the community. Reviewers will be specifically instructed to not penalize honesty concerning limitations.

3. **Theory Assumptions and Proofs**

   Question: For each theoretical result, does the paper provide the full set of assumptions and a complete (and correct) proof?

   Answer: [NA]

   Justification: Our work does not include any theoretical results.

   Guidelines:

   - The answer NA means that the paper does not include theoretical results.
   - All the theorems, formulas, and proofs in the paper should be numbered and cross-referenced.
   - All assumptions should be clearly stated or referenced in the statement of any theorems.
   - The proofs can either appear in the main paper or the supplemental material, but if they appear in the supplemental material, the authors are encouraged to provide a short proof sketch to provide intuition.
   - Inversely, any informal proof provided in the core of the paper should be complemented by formal proofs provided in appendix or supplemental material.
   - Theorems and Lemmas that the proof relies upon should be properly referenced.

4. **Experimental Result Reproducibility**

   Question: Does the paper fully disclose all the information needed to reproduce the main experimental results of the paper to the extent that it affects the main claims and/or conclusions of the paper (regardless of whether the code and data are provided or not)?

   Answer: [Yes]

   Justification: We provided all information for reproducibility of the experiment.

   Guidelines:

- The answer NA means that the paper does not include experiments.
- If the paper includes experiments, a No answer to this question will not be perceived well by the reviewers: Making the paper reproducible is important, regardless of whether the code and data are provided or not.
- If the contribution is a dataset and/or model, the authors should describe the steps taken to make their results reproducible or verifiable.
- Depending on the contribution, reproducibility can be accomplished in various ways. For example, if the contribution is a novel architecture, describing the architecture fully might suffice, or if the contribution is a specific model and empirical evaluation, it may be necessary to either make it possible for others to replicate the model with the same dataset, or provide access to the model. In general. releasing code and data is often one good way to accomplish this, but reproducibility can also be provided via detailed instructions for how to replicate the results, access to a hosted model (e.g., in the case of a large language model), releasing of a model checkpoint, or other means that are appropriate to the research performed.
- While NeurIPS does not require releasing code, the conference does require all submissions to provide some reasonable avenue for reproducibility, which may depend on the nature of the contribution. For example
  (a) If the contribution is primarily a new algorithm, the paper should make it clear how to reproduce that algorithm.
  (b) If the contribution is primarily a new model architecture, the paper should describe the architecture clearly and fully.
  (c) If the contribution is a new model (e.g., a large language model), then there should either be a way to access this model for reproducing the results or a way to reproduce the model (e.g., with an open-source dataset or instructions for how to construct the dataset).
  (d) We recognize that reproducibility may be tricky in some cases, in which case authors are welcome to describe the particular way they provide for reproducibility. In the case of closed-source models, it may be that access to the model is limited in some way (e.g., to registered users), but it should be possible for other researchers to have some path to reproducing or verifying the results.

5. **Open access to data and code**

   Question: Does the paper provide open access to the data and code, with sufficient instructions to faithfully reproduce the main experimental results, as described in supplemental material?

   Answer: [Yes]

   Justification: We release our code in `https://github.com/esw0116/ODGS` to facilitate the related research.

   Guidelines:

   - The answer NA means that paper does not include experiments requiring code.
   - Please see the NeurIPS code and data submission guidelines (`https://nips.cc/public/guides/CodeSubmissionPolicy`) for more details.
   - While we encourage the release of code and data, we understand that this might not be possible, so "No" is an acceptable answer. Papers cannot be rejected simply for not including code, unless this is central to the contribution (e.g., for a new open-source benchmark).
   - The instructions should contain the exact command and environment needed to run to reproduce the results. See the NeurIPS code and data submission guidelines (`https://nips.cc/public/guides/CodeSubmissionPolicy`) for more details.
   - The authors should provide instructions on data access and preparation, including how to access the raw data, preprocessed data, intermediate data, and generated data, etc.
   - The authors should provide scripts to reproduce all experimental results for the new proposed method and baselines. If only a subset of experiments are reproducible, they should state which ones are omitted from the script and why.

- At submission time, to preserve anonymity, the authors should release anonymized versions (if applicable).
- Providing as much information as possible in supplemental material (appended to the paper) is recommended, but including URLs to data and code is permitted.

6. **Experimental Setting/Details**

   Question: Does the paper specify all the training and test details (e.g., data splits, hyperparameters, how they were chosen, type of optimizer, etc.) necessary to understand the results?

   Answer: [Yes]

   Justification: We sufficiently describe the detailed experimental settings for preserving reproducibility. They are written in Section 4.1 and Appendix A.1. Also, we release the code to help other researchers reproduce our work.

   Guidelines:

   - The answer NA means that the paper does not include experiments.
   - The experimental setting should be presented in the core of the paper to a level of detail that is necessary to appreciate the results and make sense of them.
   - The full details can be provided either with the code, in appendix, or as supplemental material.

7. **Experiment Statistical Significance**

   Question: Does the paper report error bars suitably and correctly defined or other appropriate information about the statistical significance of the experiments?

   Answer: [No]

   Justification: We do not include error bars since each optimization is computationally heavy to compare with existing, slow method. Also, our methods and all baseline should be optimized for each scene individually, making the amount of experimentation be burdensome.

   Guidelines:

   - The answer NA means that the paper does not include experiments.
   - The authors should answer "Yes" if the results are accompanied by error bars, confidence intervals, or statistical significance tests, at least for the experiments that support the main claims of the paper.
   - The factors of variability that the error bars are capturing should be clearly stated (for example, train/test split, initialization, random drawing of some parameter, or overall run with given experimental conditions).
   - The method for calculating the error bars should be explained (closed form formula, call to a library function, bootstrap, etc.)
   - The assumptions made should be given (e.g., Normally distributed errors).
   - It should be clear whether the error bar is the standard deviation or the standard error of the mean.
   - It is OK to report 1-sigma error bars, but one should state it. The authors should preferably report a 2-sigma error bar than state that they have a 96% CI, if the hypothesis of Normality of errors is not verified.
   - For asymmetric distributions, the authors should be careful not to show in tables or figures symmetric error bars that would yield results that are out of range (e.g. negative error rates).
   - If error bars are reported in tables or plots, The authors should explain in the text how they were calculated and reference the corresponding figures or tables in the text.

8. **Experiments Compute Resources**

   Question: For each experiment, does the paper provide sufficient information on the computer resources (type of compute workers, memory, time of execution) needed to reproduce the experiments?

   Answer: [Yes]

   Justification: We describe the computational resource in Section 4.1

Guidelines:

- The answer NA means that the paper does not include experiments.
- The paper should indicate the type of compute workers CPU or GPU, internal cluster, or cloud provider, including relevant memory and storage.
- The paper should provide the amount of compute required for each of the individual experimental runs as well as estimate the total compute.
- The paper should disclose whether the full research project required more compute than the experiments reported in the paper (e.g., preliminary or failed experiments that didn't make it into the paper).

9. **Code Of Ethics**

   Question: Does the research conducted in the paper conform, in every respect, with the NeurIPS Code of Ethics `https://neurips.cc/public/EthicsGuidelines`?

   Answer: [Yes]

   Justification: Yes, we have reviewd the Neruips Code of Ethics

   Guidelines:

   - The answer NA means that the authors have not reviewed the NeurIPS Code of Ethics.
   - If the authors answer No, they should explain the special circumstances that require a deviation from the Code of Ethics.
   - The authors should make sure to preserve anonymity (e.g., if there is a special consideration due to laws or regulations in their jurisdiction).

10. **Broader Impacts**

    Question: Does the paper discuss both potential positive societal impacts and negative societal impacts of the work performed?

    Answer: [NA]

    Justification: There is no societal impacts which can be triggered from this work.

    Guidelines:

    - The answer NA means that there is no societal impact of the work performed.
    - If the authors answer NA or No, they should explain why their work has no societal impact or why the paper does not address societal impact.
    - Examples of negative societal impacts include potential malicious or unintended uses (e.g., disinformation, generating fake profiles, surveillance), fairness considerations (e.g., deployment of technologies that could make decisions that unfairly impact specific groups), privacy considerations, and security considerations.
    - The conference expects that many papers will be foundational research and not tied to particular applications, let alone deployments. However, if there is a direct path to any negative applications, the authors should point it out. For example, it is legitimate to point out that an improvement in the quality of generative models could be used to generate deepfakes for disinformation. On the other hand, it is not needed to point out that a generic algorithm for optimizing neural networks could enable people to train models that generate Deepfakes faster.
    - The authors should consider possible harms that could arise when the technology is being used as intended and functioning correctly, harms that could arise when the technology is being used as intended but gives incorrect results, and harms following from (intentional or unintentional) misuse of the technology.
    - If there are negative societal impacts, the authors could also discuss possible mitigation strategies (e.g., gated release of models, providing defenses in addition to attacks, mechanisms for monitoring misuse, mechanisms to monitor how a system learns from feedback over time, improving the efficiency and accessibility of ML).

11. **Safeguards**

    Question: Does the paper describe safeguards that have been put in place for responsible release of data or models that have a high risk for misuse (e.g., pretrained language models, image generators, or scraped datasets)?

Answer: [NA]

Justification: Our method does not include that can trigger such risks.

Guidelines:

- The answer NA means that the paper poses no such risks.
- Released models that have a high risk for misuse or dual-use should be released with necessary safeguards to allow for controlled use of the model, for example by requiring that users adhere to usage guidelines or restrictions to access the model or implementing safety filters.
- Datasets that have been scraped from the Internet could pose safety risks. The authors should describe how they avoided releasing unsafe images.
- We recognize that providing effective safeguards is challenging, and many papers do not require this, but we encourage authors to take this into account and make a best faith effort.

12. **Licenses for existing assets**

Question: Are the creators or original owners of assets (e.g., code, data, models), used in the paper, properly credited and are the license and terms of use explicitly mentioned and properly respected?

Answer: [Yes]

Justification: We explained the license of dataset in Section 4.1

Guidelines:

- The answer NA means that the paper does not use existing assets.
- The authors should cite the original paper that produced the code package or dataset.
- The authors should state which version of the asset is used and, if possible, include a URL.
- The name of the license (e.g., CC-BY 4.0) should be included for each asset.
- For scraped data from a particular source (e.g., website), the copyright and terms of service of that source should be provided.
- If assets are released, the license, copyright information, and terms of use in the package should be provided. For popular datasets, `paperswithcode.com/datasets` has curated licenses for some datasets. Their licensing guide can help determine the license of a dataset.
- For existing datasets that are re-packaged, both the original license and the license of the derived asset (if it has changed) should be provided.
- If this information is not available online, the authors are encouraged to reach out to the asset's creators.

13. **New Assets**

Question: Are new assets introduced in the paper well documented and is the documentation provided alongside the assets?

Answer: [NA]

Justification: We do not release any assets in this work.

Guidelines:

- The answer NA means that the paper does not release new assets.
- Researchers should communicate the details of the dataset/code/model as part of their submissions via structured templates. This includes details about training, license, limitations, etc.
- The paper should discuss whether and how consent was obtained from people whose asset is used.
- At submission time, remember to anonymize your assets (if applicable). You can either create an anonymized URL or include an anonymized zip file.

14. **Crowdsourcing and Research with Human Subjects**

Question: For crowdsourcing experiments and research with human subjects, does the paper include the full text of instructions given to participants and screenshots, if applicable, as well as details about compensation (if any)?

Answer: [NA]

Justification: We do not include any crowdsourcing or research related to human subjects.

Guidelines:

- The answer NA means that the paper does not involve crowdsourcing nor research with human subjects.
- Including this information in the supplemental material is fine, but if the main contribution of the paper involves human subjects, then as much detail as possible should be included in the main paper.
- According to the NeurIPS Code of Ethics, workers involved in data collection, curation, or other labor should be paid at least the minimum wage in the country of the data collector.

15. **Institutional Review Board (IRB) Approvals or Equivalent for Research with Human Subjects**

Question: Does the paper describe potential risks incurred by study participants, whether such risks were disclosed to the subjects, and whether Institutional Review Board (IRB) approvals (or an equivalent approval/review based on the requirements of your country or institution) were obtained?

Answer: [NA]

Justification: We do not include any crowdsourcing or research related to human subjects.

Guidelines:

- The answer NA means that the paper does not involve crowdsourcing nor research with human subjects.
- Depending on the country in which research is conducted, IRB approval (or equivalent) may be required for any human subjects research. If you obtained IRB approval, you should clearly state this in the paper.
- We recognize that the procedures for this may vary significantly between institutions and locations, and we expect authors to adhere to the NeurIPS Code of Ethics and the guidelines for their institution.
- For initial submissions, do not include any information that would break anonymity (if applicable), such as the institution conducting the review.